[redacted]

Copy 237
RM L54L31b

NACA RM L54L31b

TECH LIBRARY KAFB, NM
0144231

7597

NACA

RESEARCH MEMORANDUM

TRANSONIC WIND-TUNNEL INVESTIGATION OF THE EFFECTS OF SWEEPBACK AND THICKNESS RATIO ON THE WING LOADS OF A WING-BODY COMBINATION OF ASPECT RATIO 4 AND TAPER RATIO 0.6

By Robert J. Platt, Jr., and Joseph D. Brooks

Langley Aeronautical Laboratory
Langley Field, Va.

[redacted]

NATIONAL ADVISORY COMMITTEE
FOR AERONAUTICS
WASHINGTON
April 4, 1955

[redacted]

[redacted]

sections measured parallel to the plane of symmetry. An additional unswept wing with NACA 65A004 airfoil sections was tested to provide information on thickness effects.

Normal force, pitching moment, and wing-root bending moment of the wings were measured by means of a strain-gage balance. From these measurements, the location of the center of pressure on the wing was computed.

SYMBOLS

a	distance from leading edge of exposed-wing mean aerodynamic chord to 0.25 chord of mean aerodynamic chord
$b/2$	semispan of wing
$(b/2)_e$	semispan of exposed wing, measured from fuselage maximum radius
C_B	bending-moment coefficient for wing panel, $\dfrac{M_B}{q\,\frac{S}{2}\,\frac{b}{2}}$
C_{m_W}	pitching-moment coefficient for total wing in presence of body, $M_W/qS\bar{c}$
C_{N_W}	normal-force coefficient for total wing in presence of body, N_W/qS
c	section chord of wing measured parallel to plane of symmetry of model
$\bar{c}$	wing mean aerodynamic chord, $2/S\int_0^{b/2} c^2dy$
$\bar{c}_e$	wing mean aerodynamic chord for exposed wing, $\frac{2}{S_e}\int_{\text{Fuselage surface}}^{b/2} c^2dy$
M	free-stream Mach number
M_B	bending moment for a wing panel about fuselage center line

M_W pitching moment of wing in presence of body, about $0.25\bar{c}$

N_W normal force on wing in presence of body

q free-stream dynamic pressure, $\rho V^2/2$

R Reynolds number, $\rho V\bar{c}/\mu$

S total wing area

S_e area of exposed wing

t maximum section thickness

V free-stream velocity

$(x/c)_{\bar{c}}$ longitudinal location of center of pressure in terms of mean aerodynamic chord, measured from leading edge of mean aerodynamic chord, $0.25 - \frac{C_{m_W}}{C_{N_W}}$

$(x/c)_{\bar{c}_e}$ longitudinal location of center of pressure in terms of exposed-wing mean aerodynamic chord, measured from leading edge of exposed-wing mean aerodynamic chord, $\frac{a}{\bar{c}_e} - \frac{\bar{c}}{\bar{c}_e}\frac{C_{m_W}}{C_{N_W}}$

$y/b/2$ lateral location of center of pressure, in terms of wing semispan, measured from fuselage center line, $\frac{C_B}{C_{N_W}}$

$(y/b/2)_e$ lateral location of center of pressure, in terms of exposed wing semispan, measured from fuselage maximum radius, $\frac{b}{b_e}\left(\frac{C_B}{C_{N_W}} - 1\right) + 1$

α angle of attack of model measured from fuselage center line, deg

$\Lambda_{c/4}$ sweepback angle of wing quarter-chord line, deg

μ coefficient of viscosity in free stream

ρ mass density in free stream

APPARATUS AND METHODS

Tunnel

The test section of the Langley 8-foot transonic pressure tunnel is rectangular in cross section. The upper and lower walls of the test section are slotted to allow continuous operation through the transonic speed range. Some details of the test section are shown in figure 1. The sting support system shown in figure 1 was designed to keep the model near the center line of the tunnel throughout the angle-of-attack range.

During this investigation, the tunnel was operated at approximately atmospheric stagnation pressure and the stagnation temperature was automatically controlled and held constant at 120° F. The tunnel air was dried sufficiently to lower the dew-point temperature below 0° F in order to prevent the formation of condensation shocks.

The tunnel was calibrated by means of an axial survey tube, provided with static-pressure orifices along its length, which extended from the entrance cone to the beginning of the diffuser. Some representative axial Mach number distributions at the center of the tunnel are shown in figure 2. The flow in the vicinity of the wing was satisfactorily uniform at all test Mach numbers. Local deviations from the average stream Mach number were no larger than 0.005 at subsonic speeds. With increases in Mach number above 1.0, these deviations increased but did not exceed 0.010 in the region of the wing at the highest test Mach number of 1.20.

Models

The plan forms of the wings tested and their dimensions are shown in figure 3. The three wings of the sweep series all had NACA 65A006 airfoil sections parallel to the plane of symmetry, an area of 1 square foot, an aspect ratio of 4, and a taper ratio of 0.6. The sweepback angles investigated were 0°, 35°, and 45° measured from the 25-percent chord line. A fourth wing, identical to the wing with 0° sweepback except that it had NACA 65A004 airfoil sections, was tested to provide information on thickness effects. The wings were constructed of aluminum alloy except for the wing with a sweepback angle of 45° which was constructed of steel.

The fuselage frame was constructed of steel and contained a strain-gage balance designed to measure wing loads independently of any body load. The balance measured bending moment on each wing and normal force and pitching moment for both wings. The wings were mounted in the balance, as shown in figure 4 and the detail of figure 3, and were independent of the body frame. A photograph of the complete model, in this case with an unswept wing, is shown in figure 5. The ordinates of the body are given in Table I.

A gap of about 0.030 inch was left between the outer body shell and the wing to prevent fouling of the wing on the body. For the tests of the unswept wings, this gap was not sealed. For the swept wings, however, because of the possibility that leakage through the gap might affect the spanwise flow along the wing and the formation of the leading-edge vortex, the gap between the outer-body shell and the wing was sealed with soft rubber tubing as shown in the detail of figure 3. For all tests the hollow sting was plugged at the base of the model to prevent any flow through the sting. The addition of the rubber seals decreased the strain-gage balance sensitivity as much as 5 percent. For this reason, the balance was recalibrated before the test of each sealed configuration.

The angle of attack was measured by a strain-gage attitude transmitter. The instrument was mounted in the body frame ahead of the wing.

Tests

The angle-of-attack range extended in most cases from 0° to 20° unless limited by the maximum allowable load on either the wing or the strain-gage balance or by severe buffeting. In the case of the thinner straight wing, the angle of attack was limited to 8° at all Mach numbers above 0.60. The Mach number range extended from 0.60 to 1.20. Data were not recorded in the Mach number range between 1.03 and 1.12 since in this range the data may have been affected by reflections of the fuselage bow wave from the tunnel walls. The variation of Reynolds number (based on a mean aerodynamic chord of 6.125 in.) with Mach number is shown in figure 6.

Accuracy

The accuracy of the strain-gage measurements is estimated to be as follows:

M	Accuracy of -		
	C_{N_W}	C_{m_W}	C_B
0.6	±0.009	±0.004	±0.008
1.2	±0.004	±0.002	±0.004

The average stream Mach number was held within ±0.003 of the nominal value given in the figures. The model angle of attack is estimated to be correct within ±0.1°.

As previously mentioned, the two straight wings were tested with an unsealed gap between the wing and body shell. The effect of such a gap was investigated for two wings with 45° sweepback and is shown in reference 1. For these wings, the data obtained with and without the seal were generally in good agreement at angles of attack below where pitch-up occurred.

During the present test, a cathetometer, sighted on the chord line of the wing tip, was used to measure the twist of the wings under load. The maximum wing tip twist measured on the four wings was as follows:

Sweep, Λ, deg	Airfoil section	Maximum twist, deg
0	NACA 65A006	0.7
35	NACA 65A006	-2.0
45	NACA 65A006	-1.0
0	NACA 65A004	1.3

No corrections to the data for aeroelastic effects have been made.

The longitudinal and lateral position of the center of pressure on the wings was computed from faired curves of C_{m_W} against C_{N_W} and

C_B against C_{N_W}, respectively. At some Mach numbers, these curves did not pass through the origin. Since the models were symmetrical, the curves were shifted to pass through the origin when computing the center-of-pressure locations. This procedure improved the accuracy of the computed center-of-pressure locations at low values of wing normal-force coefficient.

RESULTS AND DISCUSSION

Basic Aerodynamic Characteristics

The variation of angle of attack, pitching-moment coefficient and bending-moment coefficient with wing normal-force coefficient for the 6-percent-thick wings with sweepback angles of 0°, 35°, 45°, and the 4-percent-thick unswept wing are presented in figures 7, 8, 9, and 10, respectively. The force and moment coefficients shown were measured on the wings in the presence of the body. In figures 7(c), 8(c), 9(c), and 10(c), bending-moment coefficients for both left- and right-wing panels are shown, flags on the symbols serving to identify the left-wing panel moment.

In the case of the 6-percent-thick unswept wing (fig. 7(c)), stalling apparently occurred earlier on one wing panel than on the other at Mach numbers 0.60 to 0.91. In such cases, the curves were not faired past the point where stall first occurred.

The variation of pitching-moment coefficient with normal-force coefficient for the sweptback wings (figs. 8(b) and 9(b)) indicates that pitch-up occurred at most test Mach numbers. With increasing Mach number, pitch-up is, in general, delayed to higher normal-force coefficients.

Basic Center-of-Pressure Characteristics

The longitudinal and lateral variation of the center of pressure with Mach number and normal-force coefficient is presented in figures 11 to 18 for the four test configurations. The data of figures 11, 13, 15, and 17 indicate that, with increasing Mach number, a generally rearward and outward movement of the center of pressure occurs. This shift in center of pressure is due to the development of supersonic flow on the upper surface of the wing at transonic speeds. The lateral movement of the center of pressure for the unswept wings differs from that of the swept wings in that, as the Mach number approaches 1.0, the center of pressure returns inboard slightly.

The effect of normal-force coefficient on the center of pressure is shown in figures 12, 14, 16, and 18. These data indicate that, as the normal-force coefficient increases at a constant Mach number, the center-of-pressure movement is generally rearward until, in the case of the sweptback wings, pitch-up occurs and the center of pressure then moves forward and inboard.

Effect of Sweepback on Center of Pressure

If the longitudinal locations of the center of pressure, in terms of the mean aerodynamic chord of the total wing area, are compared for the straight and swept wing (figs. 11 to 16), large differences may be noted. However, these differences are mainly due to the fact that a considerable portion of the wing area is blanketed by the fuselage so that a rearward displacement of the center of pressure on the swept wings results. A more logical comparison of the effects of sweepback on center-of-pressure location will result if only the portion of the wing extending beyond the fuselage is considered. Therefore, all comparisons of the longitudinal and, to be consistent, the lateral location of the center of pressure will be made with respect to the mean aerodynamic chord of the exposed wing.

At a constant normal-force coefficient, the effect of sweepback on the variation of the center-of-pressure location with Mach number is shown in figure 19. Up to a Mach number of 0.80, the center-of-pressure locations on the three wings are relatively constant. As the Mach number increases, the outward and rearward shift of the center of pressure is first noted for the straight wing. This movement is delayed to higher Mach numbers as the sweepback angle is increased. With further increases in Mach number, the center of pressure of the straight wing reversed its outward movement but the center of pressure of the swept wings continued to move outboard, the largest movement occurring on the wing with the highest sweep angle. At supersonic speeds, there was little change laterally, but longitudinally the center-of-pressure location continued to move rearward at a reduced rate up to the highest Mach number tested.

At a constant Mach number, the effect of sweepback on the variation of the center-of-pressure location with normal-force coefficient is shown in figure 20. The center of pressure of the straight wing moved rearward and slightly outboard as the normal-force coefficient increased. The center of pressure of the swept wings, in general, showed only a rearward movement preceding the forward and inboard movement that occurred at pitch-up. The data of figure 20 indicate that pitch-up occurred at a lower value of normal-force coefficient as the sweepback angle increased. However, when pitch-up did occur, the movement of the center-of-pressure was more abrupt for the 35° wing than for the 45° swept wing.

Effect of Thickness Ratio on Center of Pressure

The variation of the center-of-pressure location with Mach number, based on the exposed-wing area, is presented in figure 21 for the two unswept wings of 4-percent and 6-percent maximum thickness ratio. Decreasing the wing thickness appears to moderate the effect of Mach number on the center-of-pressure movement preceding $M = 1.0$. The rearward and outboard movement of the center of pressure occurs at a slightly higher Mach number and the lateral movement is reduced appreciably for the thinner wing.

An irregularity in the chordwise movement of the center of pressure may be noted in figure 21 in the Mach number range from 0.91 to 0.97 in the case of the 6-percent-thick wing. This reversal of the usual rearward movement has been noted in references 2 and 3. Reference 3 indicates that the irregularity is produced by the formation of a shock wave on the lower surface behind the shock on the upper surface of the wing. This relationship of the shock waves produces a region of reduced loading which shifts the center of pressure forward. The absence of any such irregularity in the case of the thinner wing (fig. 21) indicates that the phenomenon is influenced by thickness ratio and this is confirmed by the data of reference 4.

A comparison of the center-of-pressure locations for the two wings is shown in figure 22 plotted against wing normal-force coefficient. The variation of the center of pressure with normal-force coefficient is very similar for the two wings. However, the location of the center of pressure for the thinner wing is generally outboard and to the rear of that for the thicker wing.

The rather large difference in the longitudinal center-of-pressure location of the two wings at low Mach numbers and low normal-force coefficients (figs. 21 and 22) may possibly be due to inaccuracy of measurement. The forces and moments measured in this region are small and the fact that the pitching-moment coefficients, shown in figures 7(b) and 10(b), are nonlinear further increases the difficulty of accurately determining the center-of-pressure location.

Comparison With Theory

The lateral location of the center of pressure has been calculated from theoretical spanwise additional loadings for the three wing plan forms tested. The theoretical points obtained are shown in figure 23 along with the experimental center-of-pressure locations, based on the exposed wing, for the three wings of 6-percent thickness ratio. No corrections were made to the theoretical loadings for wing flexibility and fuselage interference, but only the theoretical loading outboard of the

maximum fuselage radius was considered in calculating the theoretical center of pressure. The theoretical spanwise loadings at subsonic speeds were obtained from the charts of reference 5, at supersonic speeds from the equations of reference 6 for the swept wings, and reference 7 for the unswept wing. Figure 23 indicates that at subsonic speeds the theoretical center-of-pressure positions are somewhat outboard of the experimental positions. This condition may be due in part to the fact that body interference effects were not considered in the theoretical calculations.

At supersonic speeds, the agreement between the theory and experiment is very good. The theoretical points shown were calculated at the lowest Mach numbers at which the theory of references 6 and 7 could be applied.

A similar comparison of theory and experiment in reference 1 for thin wings of 45° sweepback leads to the conclusion that the lateral center of pressure at low supersonic speeds may be predicted (below pitch-up) from the theoretical value calculated for a higher Mach number. The comparison of theory and experiment shown in figure 23 indicates that this conclusion of reference 1 may be extended to thin wings which cover a range of sweepback angles from 0° to 45°. This is justified by the good agreement of the theoretical values of center-of-pressure position with the experimental values at supersonic speeds and by the fact that little change occurred in the experimental center-of-pressure position at the points tested between a Mach number of 1.0 and 1.2.

CONCLUSIONS

An investigation of the effect of sweepback and thickness ratio on the wing loads of a wing in the presence of a body, made in the 8-foot transonic pressure tunnel, leads to the following conclusions:

1. At a constant wing normal-force coefficient: Increasing the sweepback delayed the rearward and outboard shift of the center of pressure to higher Mach numbers. Increasing the sweepback increased the magnitude of the outboard movement of the center of pressure. Approaching a Mach number of 1.0, the center of pressure of the straight wings returned inboard while that of the swept wings continued to move outboard. Above a Mach number of 1.0, there was little change in the center of pressure with increasing Mach number. Decreasing the thickness ratio of the straight wing reduced the center of pressure movement in the spanwise direction.

2. At a constant Mach number, as the normal-force coefficient increased, the movement of the center of pressure was primarily rearward

until, on the swept wings, pitch-up occurred and the center of pressure then moved forward and inboard.

3. The lateral center of pressure at low supersonic speeds can be estimated for thin wings of moderate aspect ratio from the theoretical value calculated for a higher Mach number.

Langley Aeronautical Laboratory,
National Advisory Committee for Aeronautics,
Langley Field, Va., December 23, 1954.

REFERENCES

1. Delano, James B., and Mugler, John P., Jr.: Transonic Wind-Tunnel Investigation of the Effects of Taper Ratio and Body Indentation on the Aerodynamic Loading Characteristics of a 45° Sweptback Wing in the Presence of a Body. NACA RM L54L28, 1955.

2. Knapp, Ronald J., and Jordan, Gareth H.: Wing Loads on the Bell X-1 Research Airplane (10-Percent-Thick Wing) as Determined by Pressure-Distribution Measurements in Flight at Subsonic and Transonic Speeds. NACA RM L53G14, 1953.

3. Knapp, Ronald J., and Jordan, Gareth H.: Flight-Determined Pressure Distributions Over the Wing of the Bell X-1 Research Airplane (10-Percent-Thick Wing) at Subsonic and Transonic Speeds. NACA RM L53D20, 1953.

4. Nelson, Warren H., and McDevitt, John B.: The Transonic Characteristics of 17 Rectangular, Symmetrical Wing Models of Varying Aspect Ratio and Thickness. NACA RM A51A12, 1951.

5. DeYoung, John, and Harper, Charles W.: Theoretical Symmetric Span Loading at Subsonic Speeds for Wings Having Arbitrary Plan Form. NACA Rep. 921, 1948.

6. Hannah, Margery E., and Margolis, Kenneth: Span Load Distributions Resulting From Constant Angle of Attack, Steady Rolling Velocity, Steady Pitching Velocity, and Constant Vertical Acceleration for Tapered Sweptback Wings With Streamwise Tips - Subsonic Leading Edges and Supersonic Trailing Edges. NACA TN 2831, 1952.

7. Martin, John C., and Jeffreys, Isabella: Span Load Distributions Resulting From Angle of Attack, Rolling, and Pitching for Tapered Sweptback Wings With Streamwise Tips - Supersonic Leading and Trailing Edges. NACA TN 2643, 1952.

TABLE I.- BODY COORDINATES

Station, in. from nose	Radius, in.	Station, in. from nose	Radius, in.
0	0	27.692	1.868
.225	.104	28.692	1.862
.5625	.193	29.692	1.849
1.125	.325	30.692	1.825
2.250	.542	31.692	1.789
3.375	.726	32.692	1.745
4.500	.887	33.692	1.694
6.750	1.167	34.692	1.638
9.000	1.390	35.692	1.570
11.250	1.559	36.692	1.486
13.500	1.683	36.900	1.468
15.750	1.770	37.500	1.408
18.000	1.828	38.500	1.298
20.250	1.864	39.500	1.167
22.500	1.875	40.500	1.030
26.500	1.875	41.250	.937

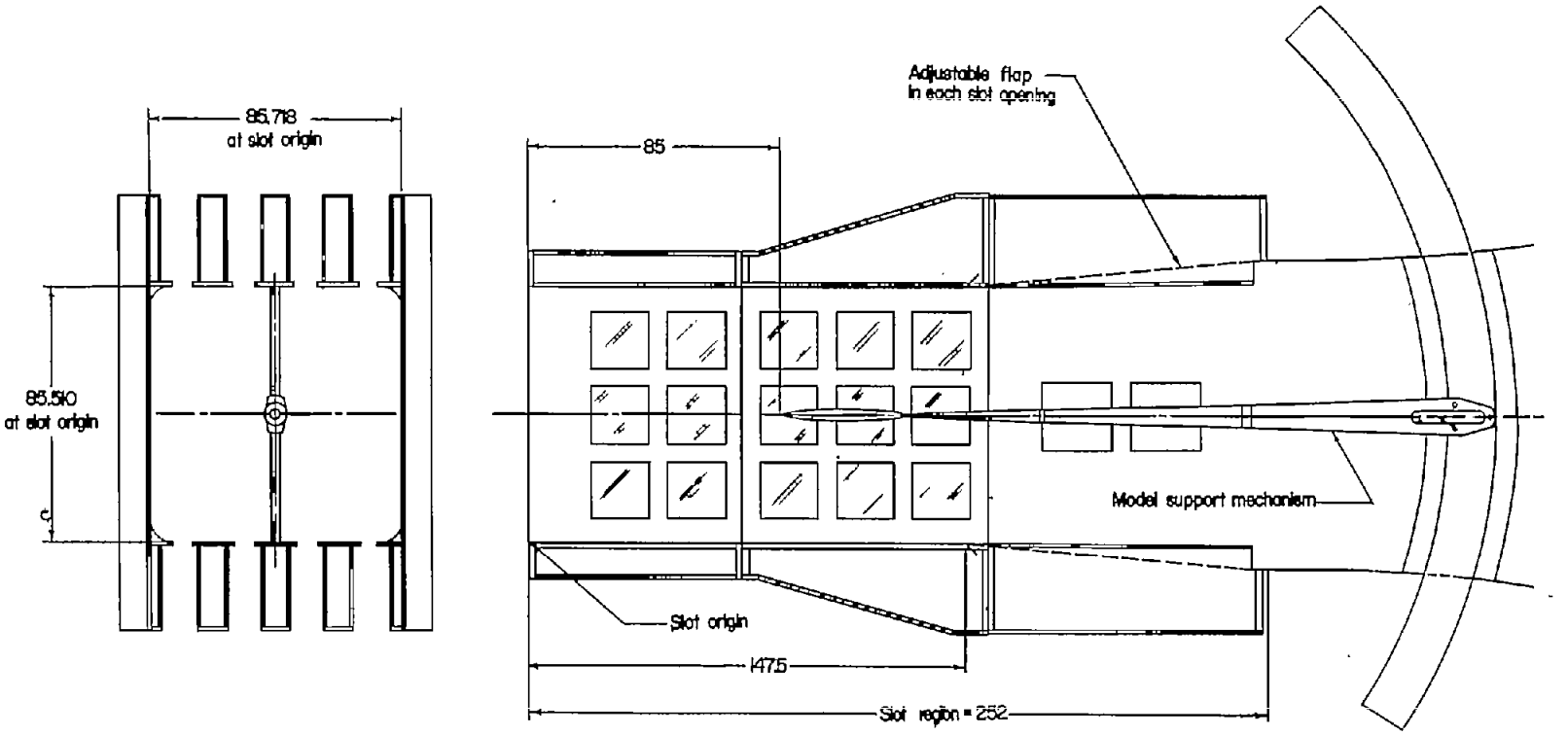

Figure 1.- Details of test section and location of model in the Langley 8-foot transonic pressure tunnel. All dimensions are in inches.

[redacted]

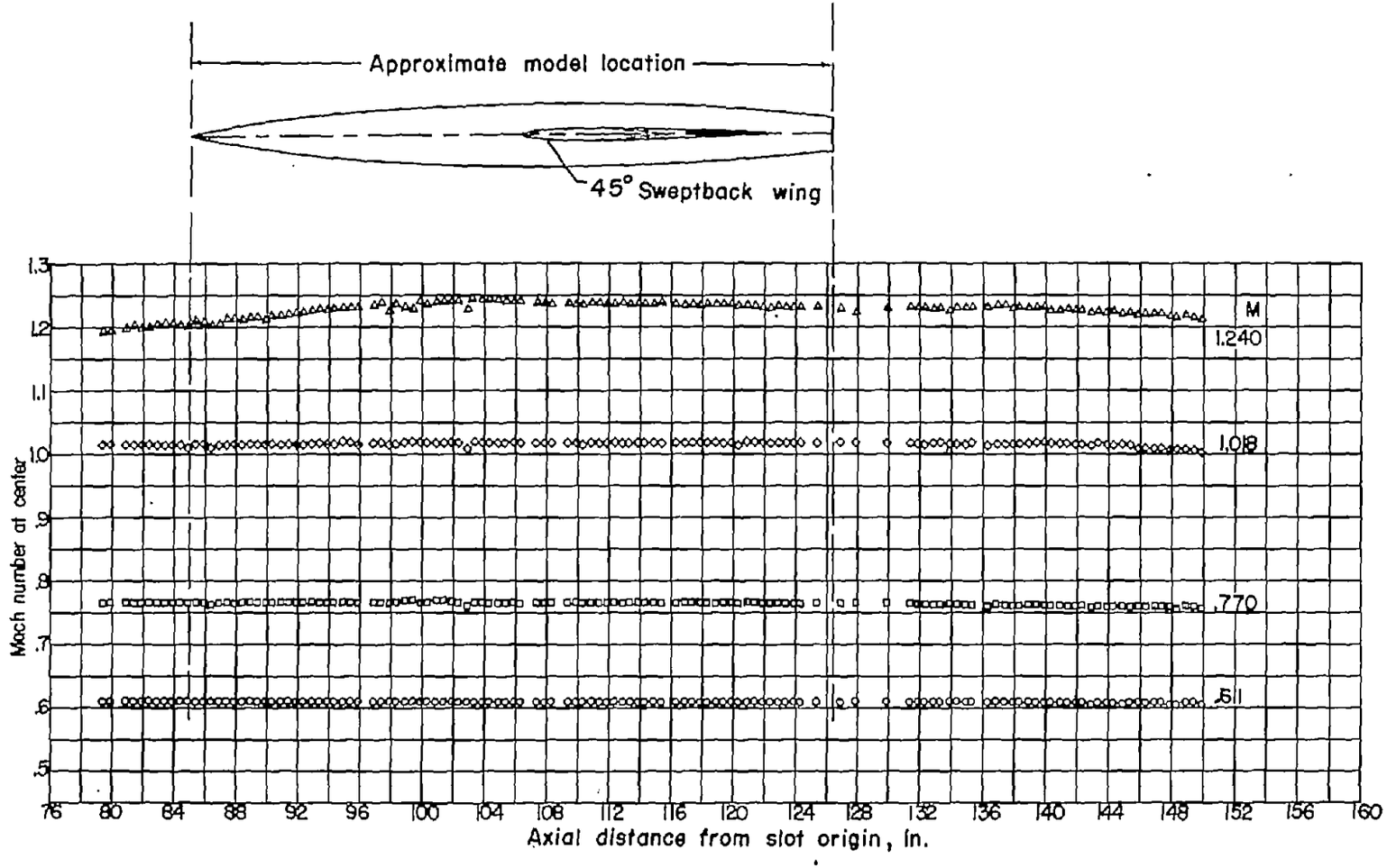

Figure 2.- Typical Mach number distributions in the test section of the Langley 8-foot transonic pressure tunnel during this investigation.

[redacted]

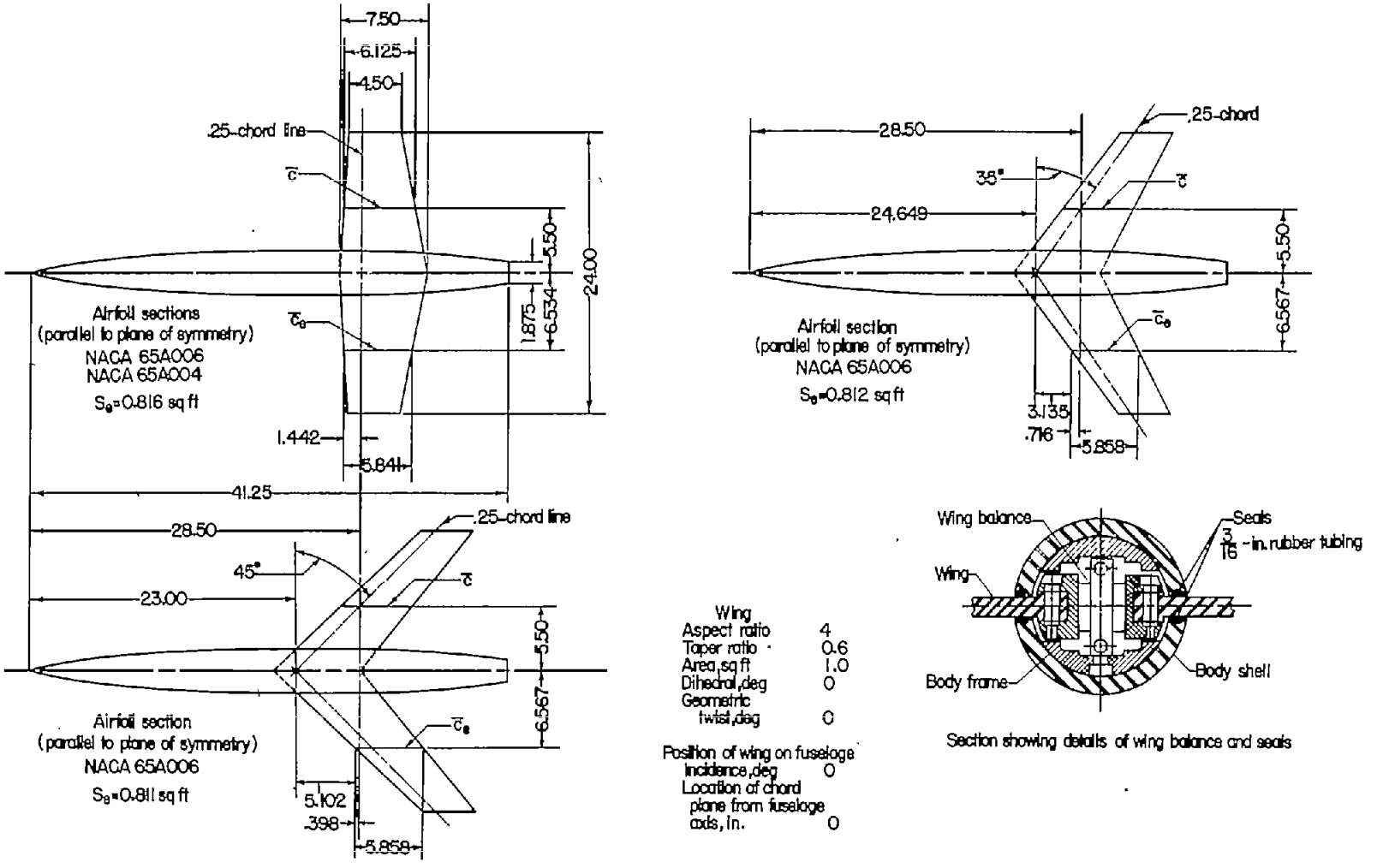

Wing	
Aspect ratio	4
Taper ratio	0.6
Area, sq ft	1.0
Dihedral, deg	0
Geometric twist, deg	0
Position of wing on fuselage	
Incidence, deg	0
Location of chord plane from fuselage axis, in.	0

Figure 3.- Wing-body configurations tested. All dimensions are in inches except as noted.

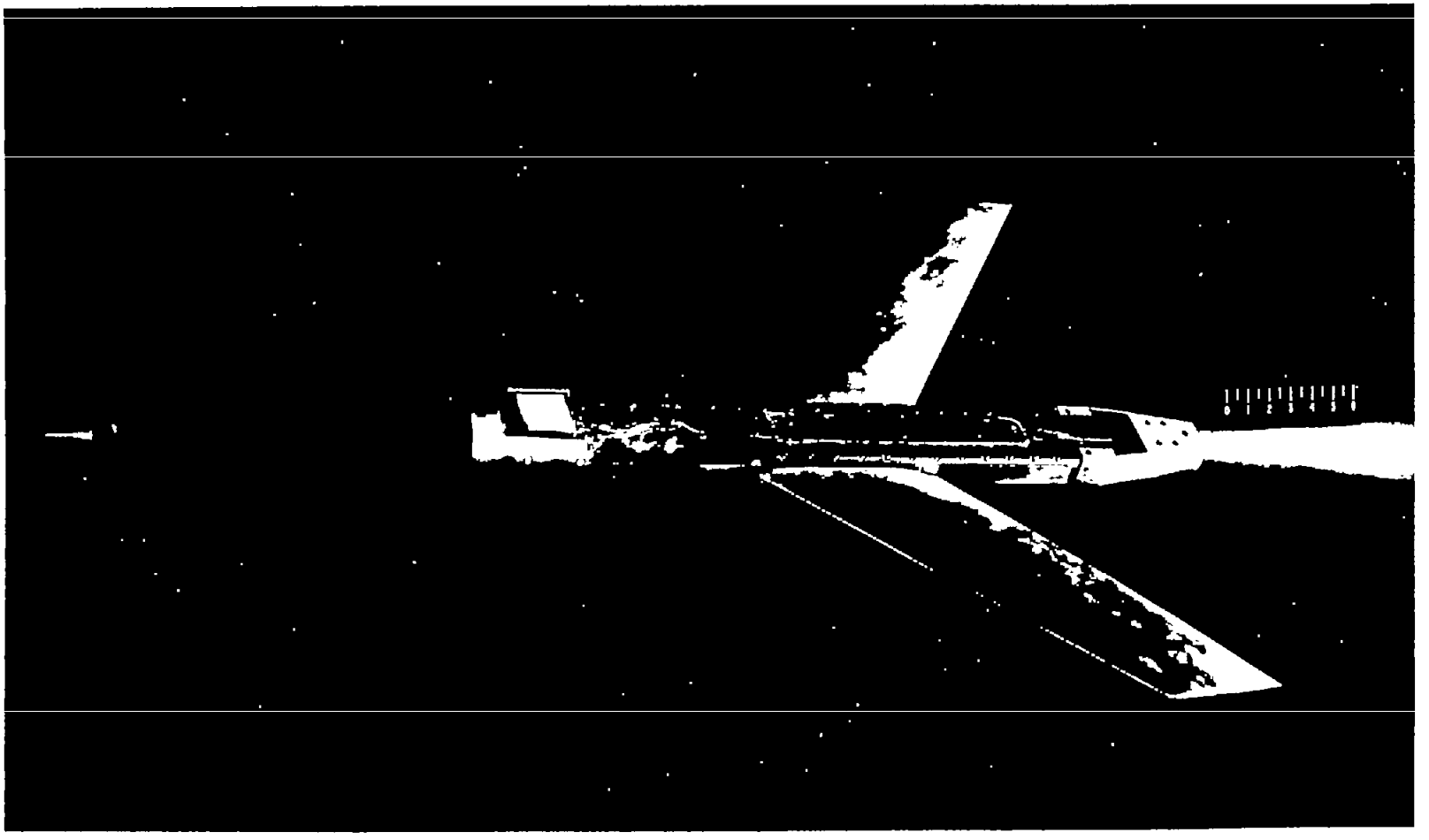

L-84808

Figure 4.- Photograph of model showing strain-gage balance.

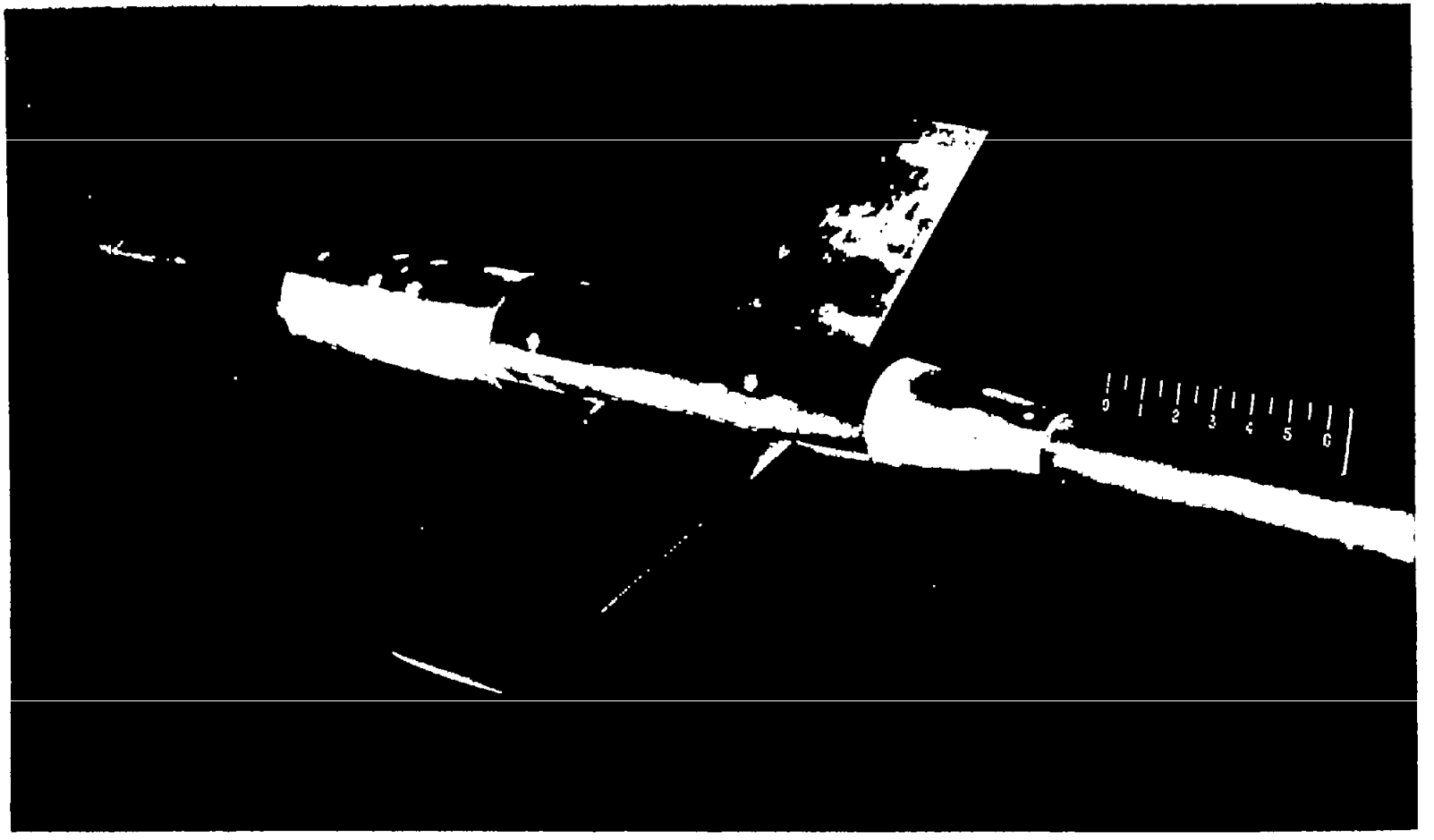

L-84817

Figure 5.- Photograph of complete model.

[redacted]

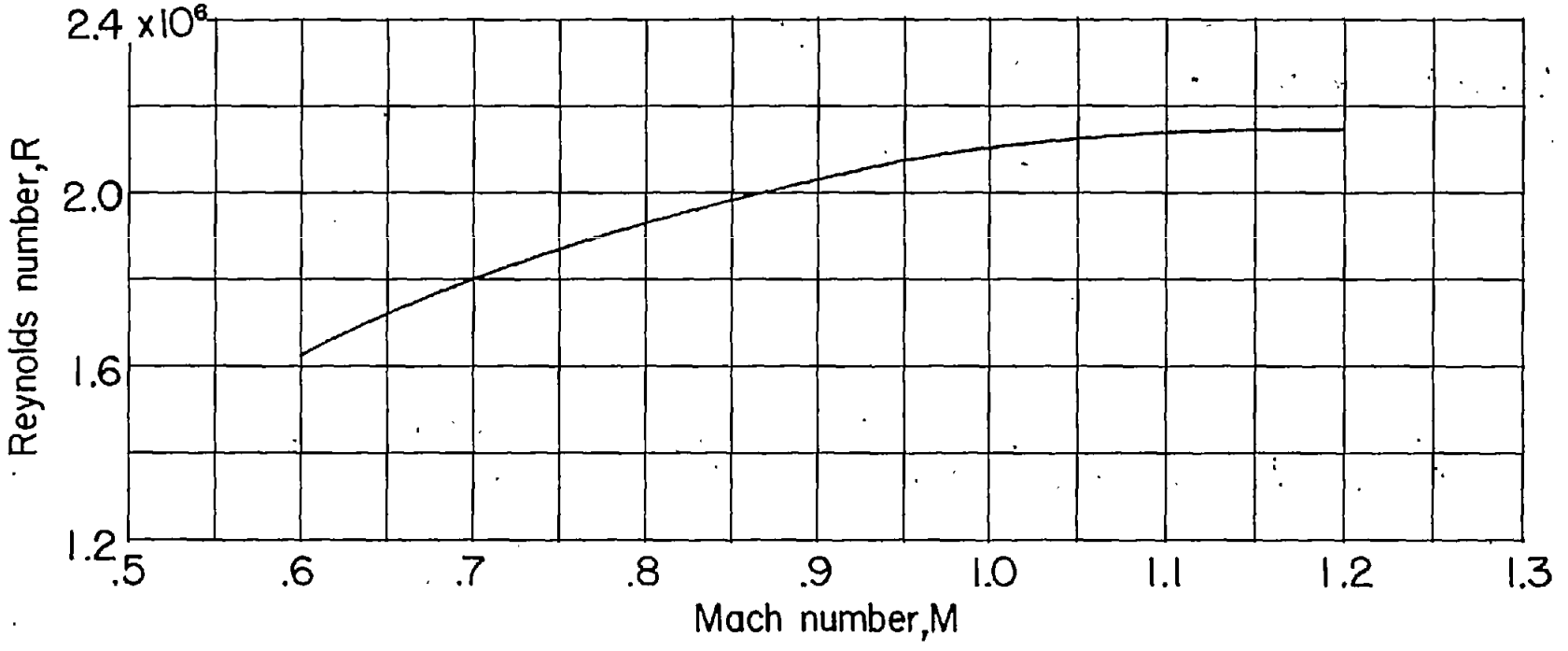

Figure 6.- Variation of Reynolds number with Mach number.

[redacted]

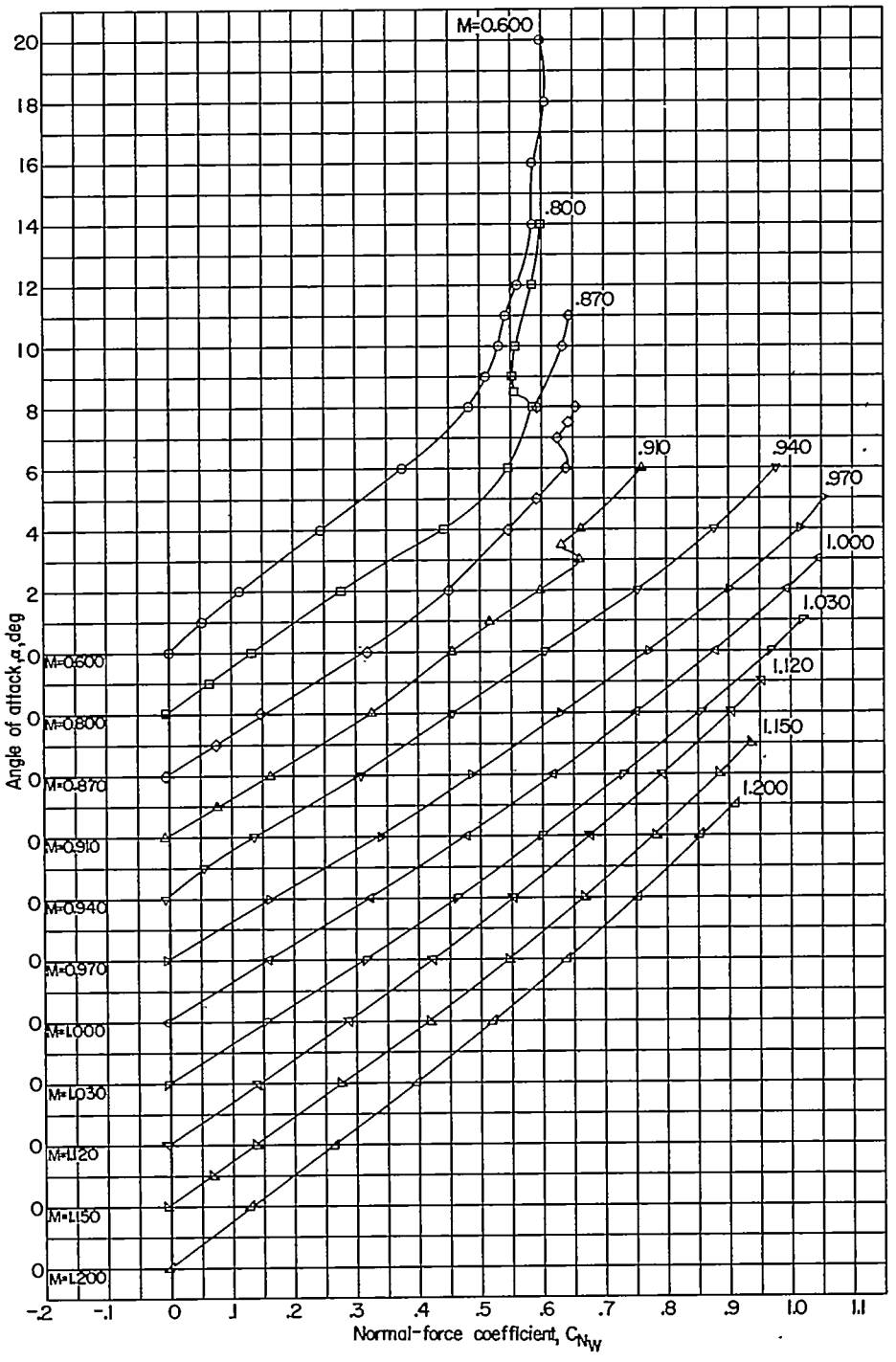

(a) Variation of α with C_{N_W}.

Figure 7.- Aerodynamic characteristics of the wing of a wing-body combination. 0° quarter-chord sweep; NACA 65A006 airfoil section.

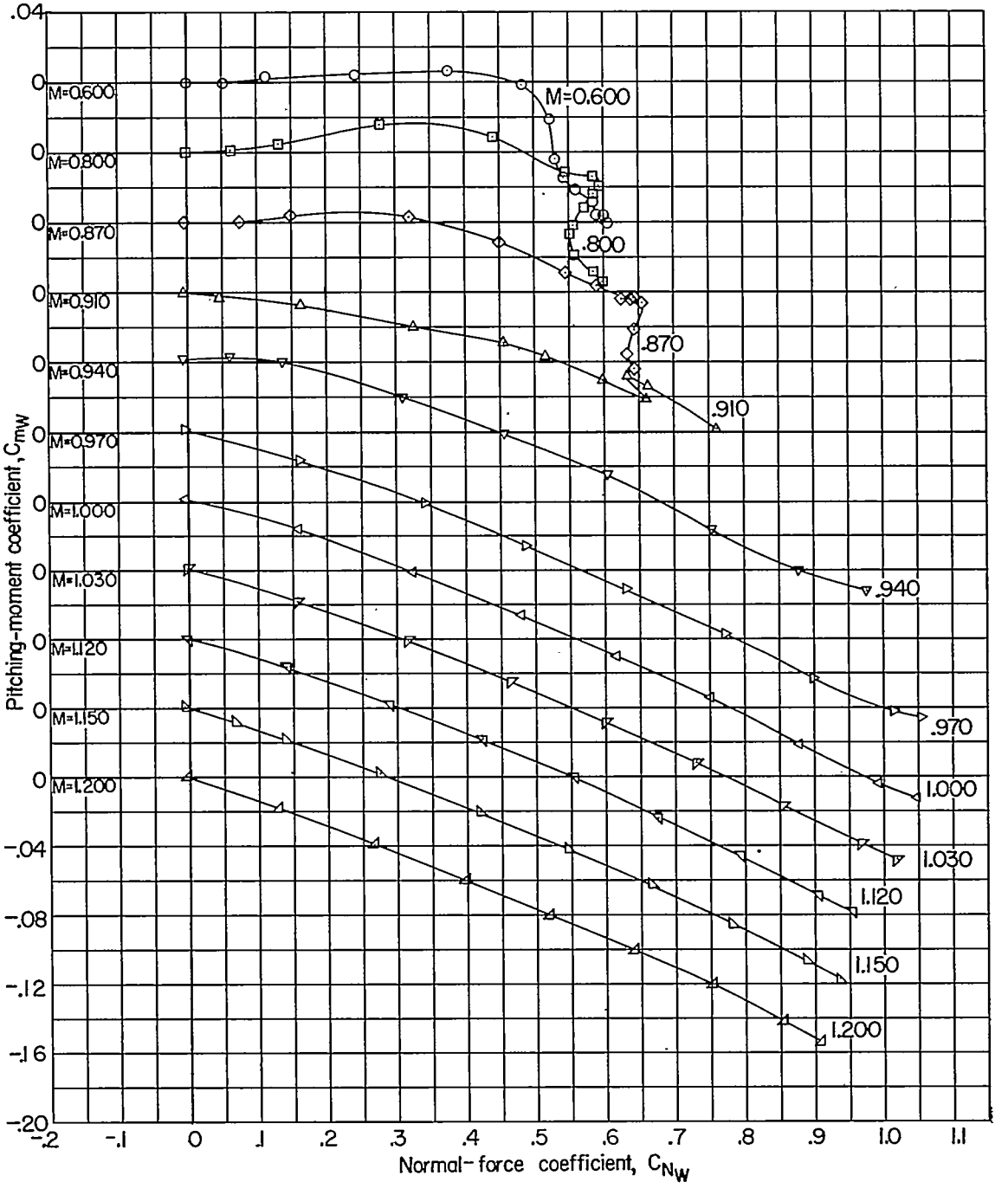

(b) Variation of C_{m_W} with C_{N_W}.

Figure 7.- Continued.

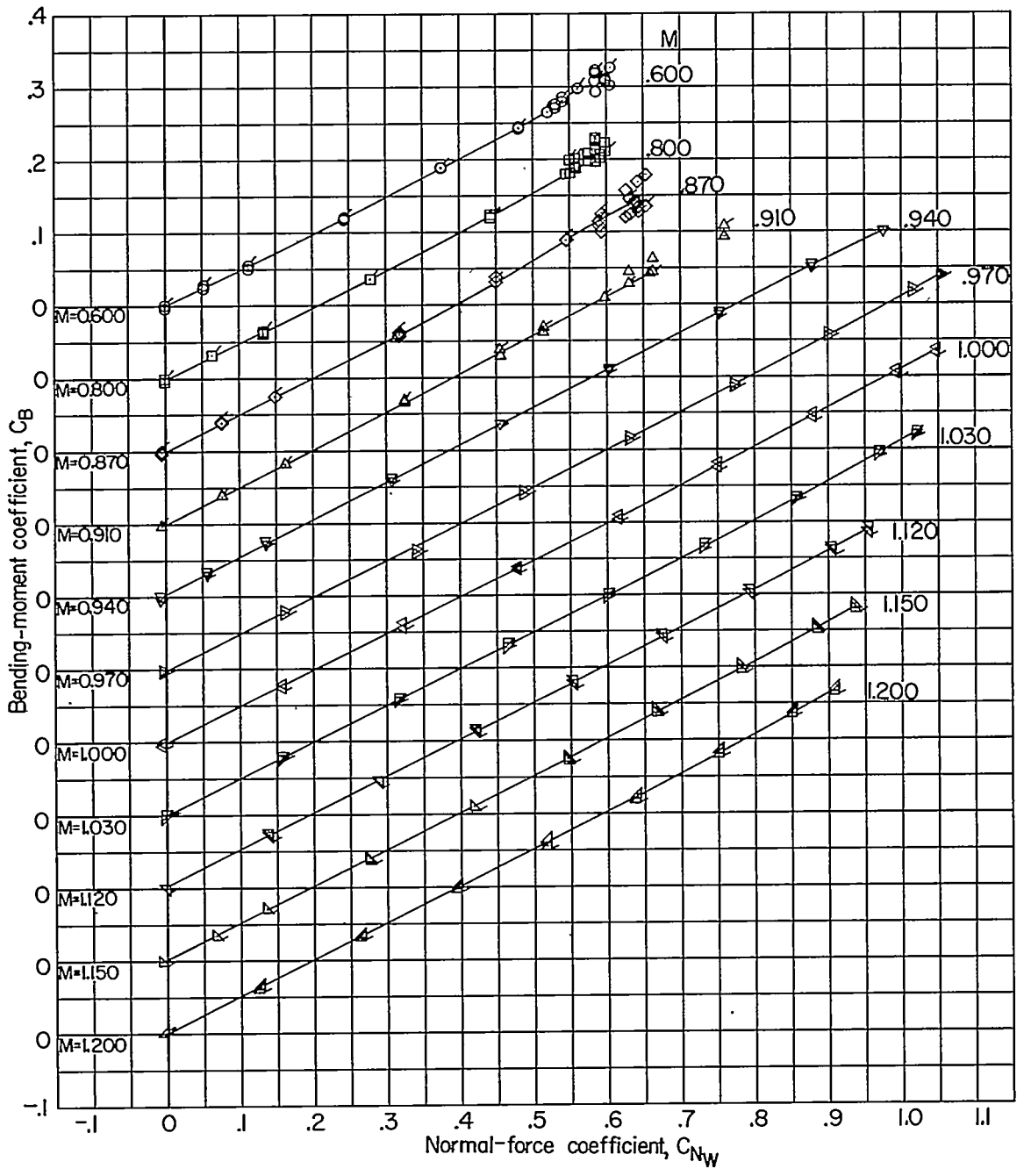

(c) Variation of C_B with C_{N_W} for left and right wing panels. Flagged symbols indicate left-wing panel.

Figure 7.- Concluded.

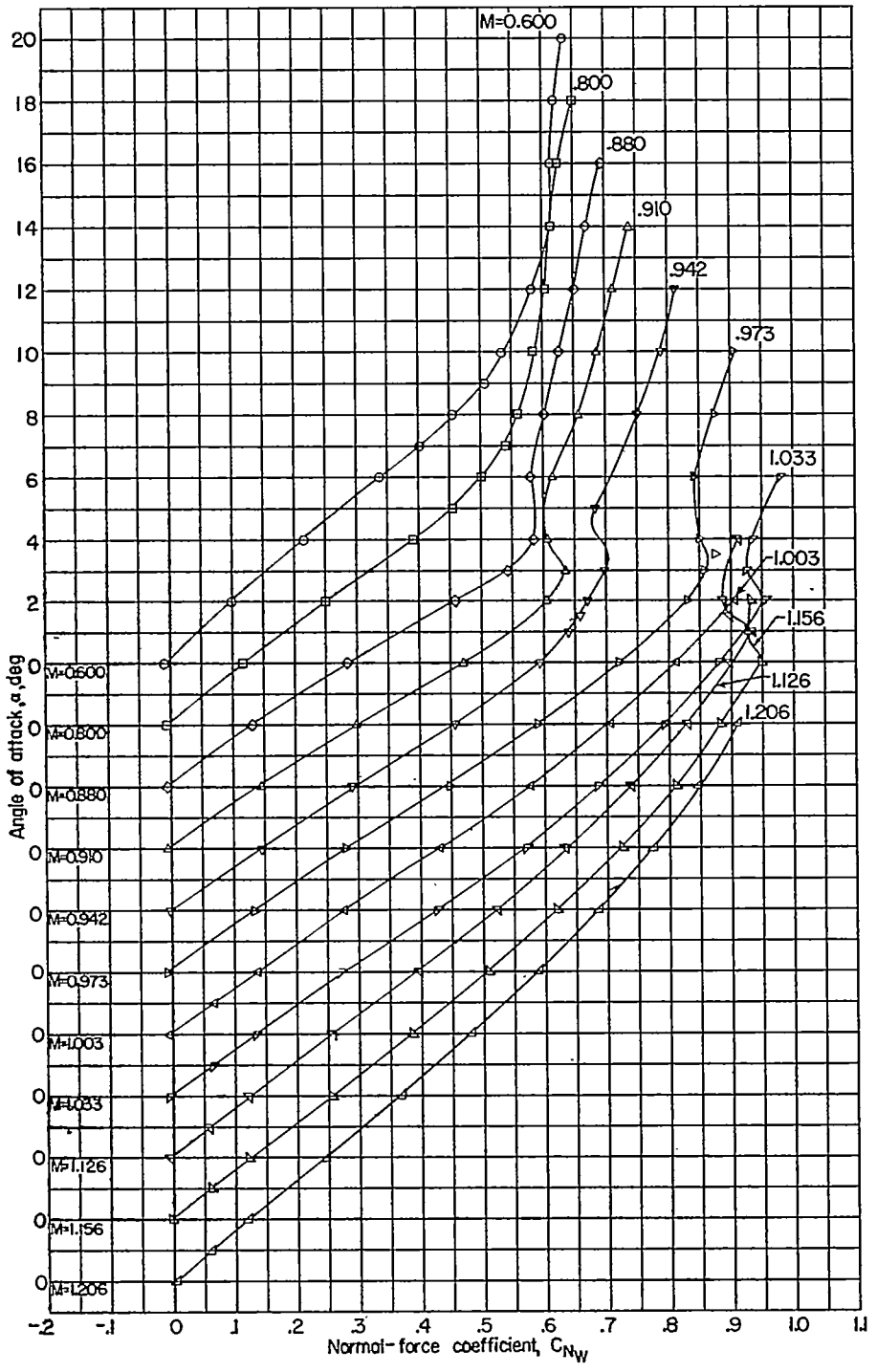

(a) Variation of α with C_{N_W}.

Figure 8.- Aerodynamic characteristics of the wing of a wing-body combination. 35° quarter-chord sweep; NACA 65A006 airfoil section.

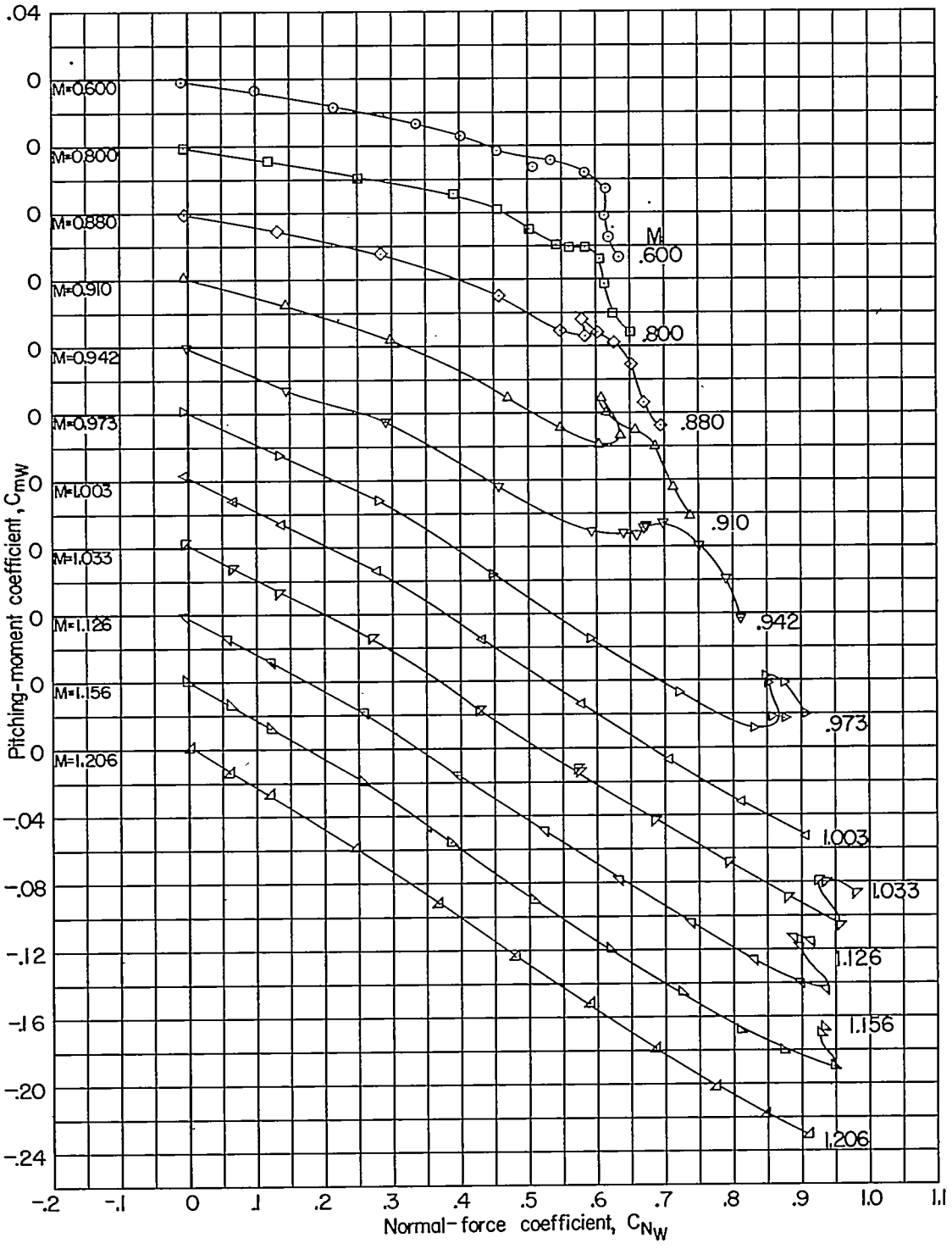

(b) Variation of C_{m_W} with C_{N_W}.

Figure 8.- Continued.

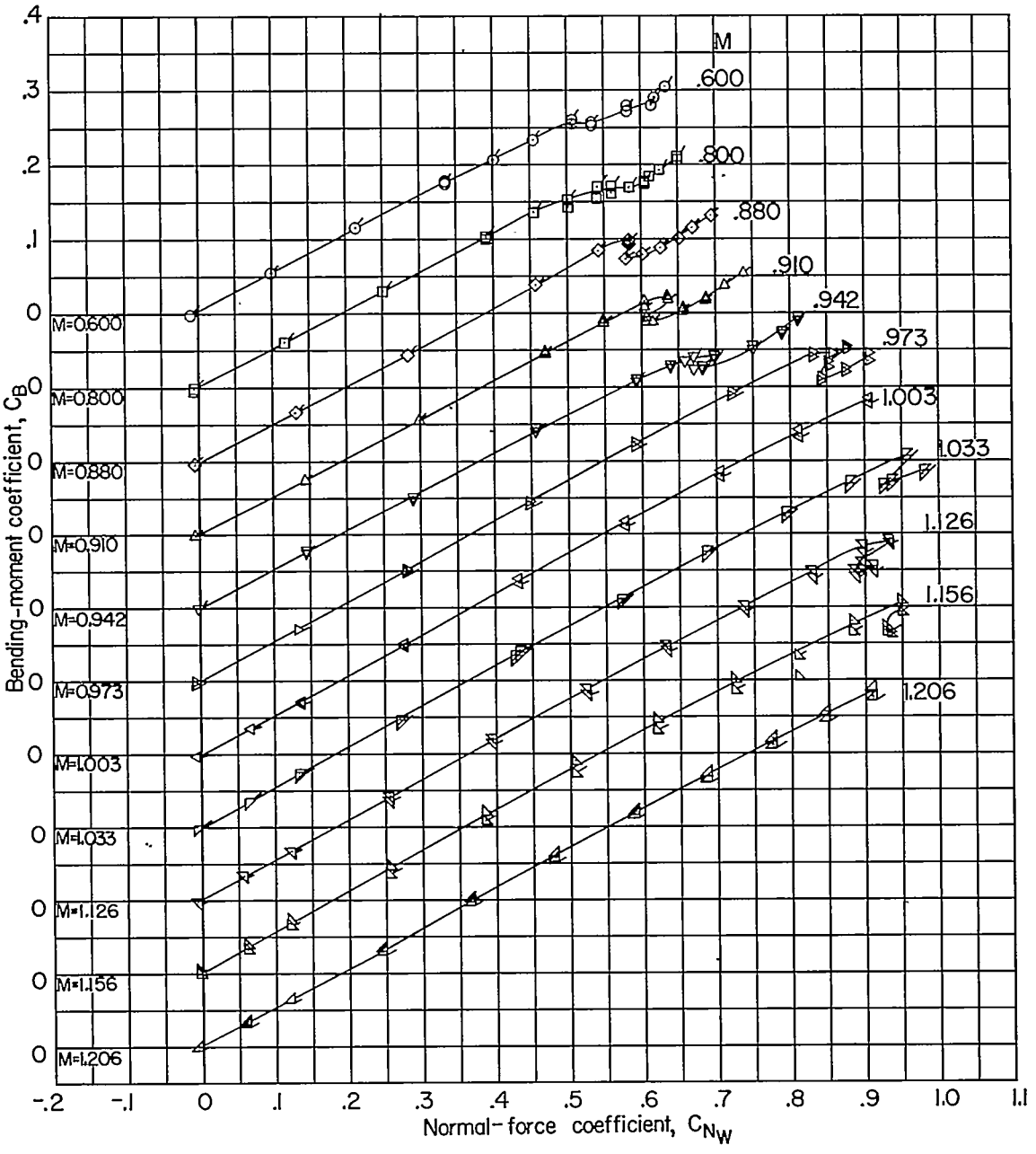

(c) Variation of C_B with C_{N_W} for left- and right-wing panels. Flagged symbols indicate left-wing panel.

Figure 8.- Concluded.

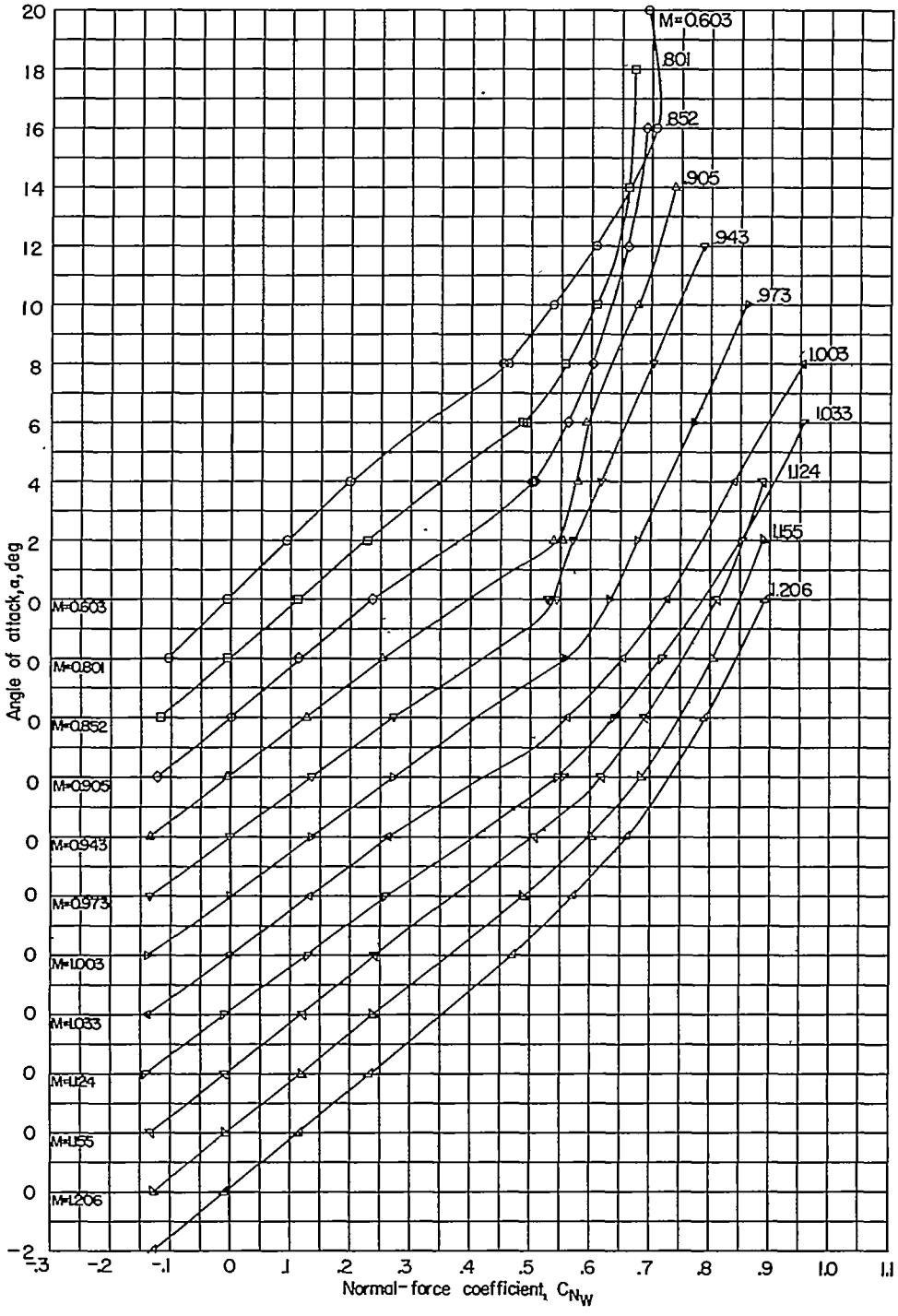

(a) Variation of α with C_{N_W}.

Figure 9.- Aerodynamic characteristics of the wing of a wing-body combination. 45° quarter-chord sweep; NACA 65A006 airfoil section.

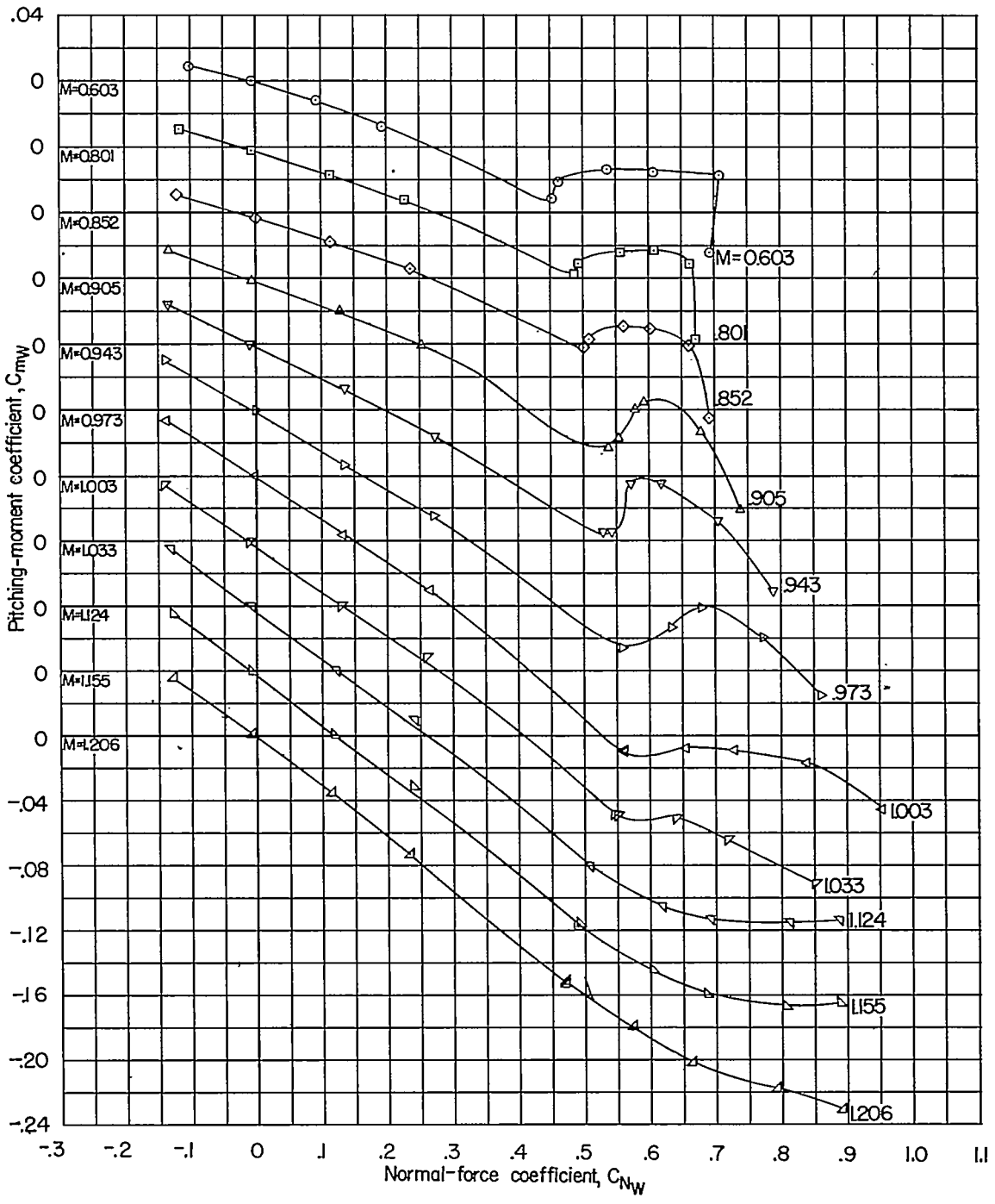

(b) Variation of C_{m_W} with C_{N_W}.

Figure 9.- Continued.

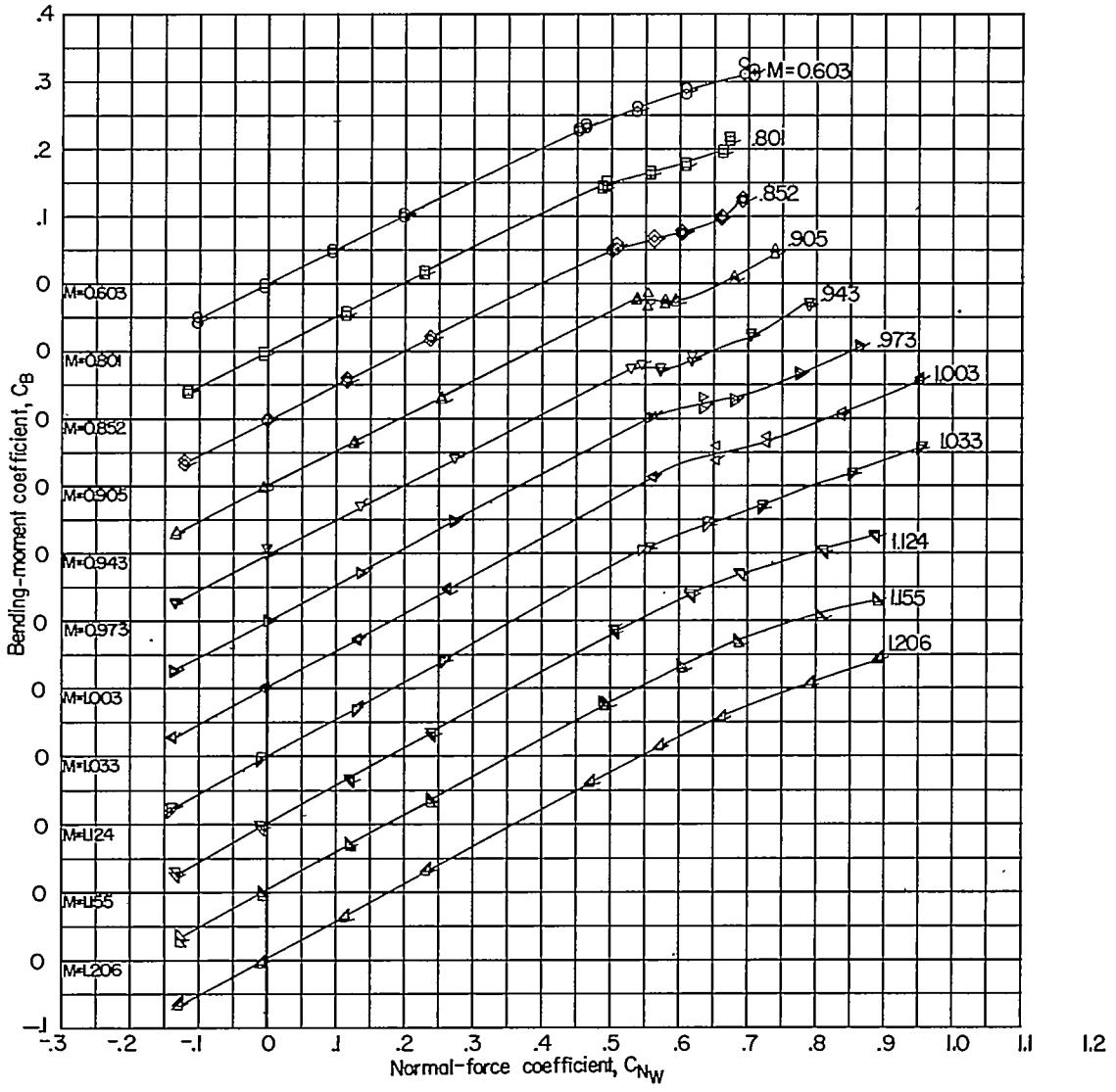

(c) Variation of C_B with C_{N_W} for left- and right-wing panels. Flagged symbols indicate left wing panel.

Figure 9.- Concluded.

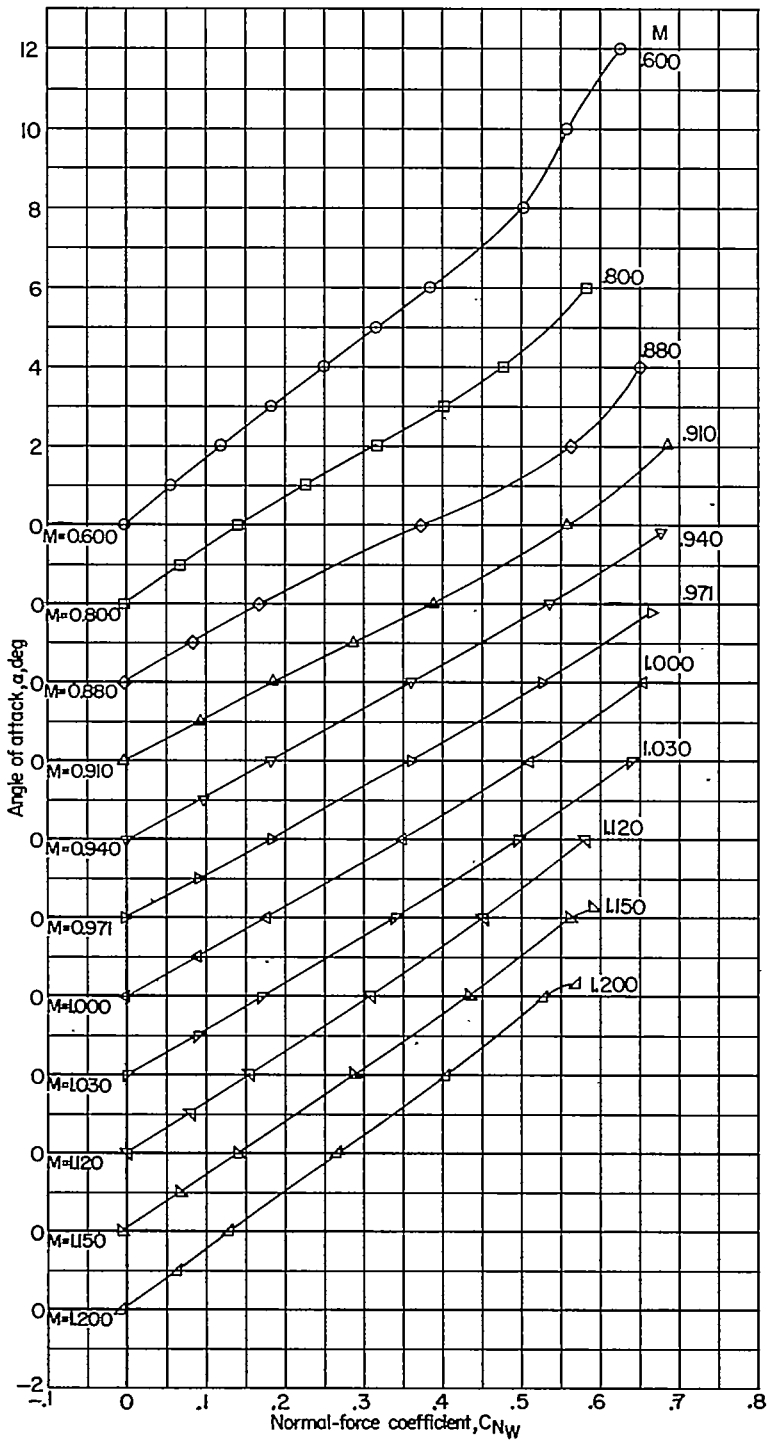

(a) Variation of α with C_{N_W}.

Figure 10.- Aerodynamic characteristics of the wing of a wing-body combination. 0° quarter-chord sweep; NACA 65A004 airfoil section.

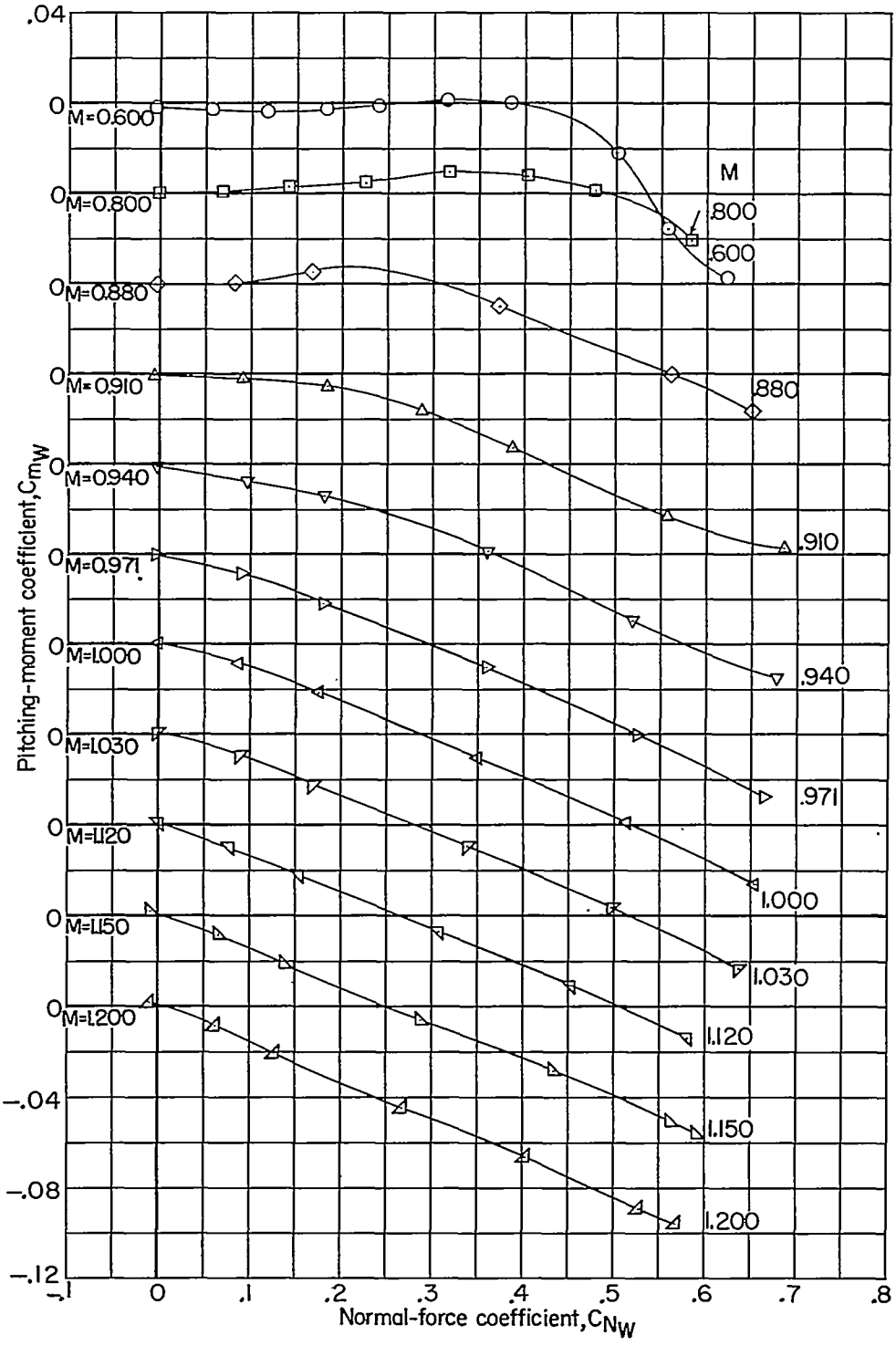

(b) Variation of C_{m_W} with C_{N_W}.

Figure 10.- Continued.

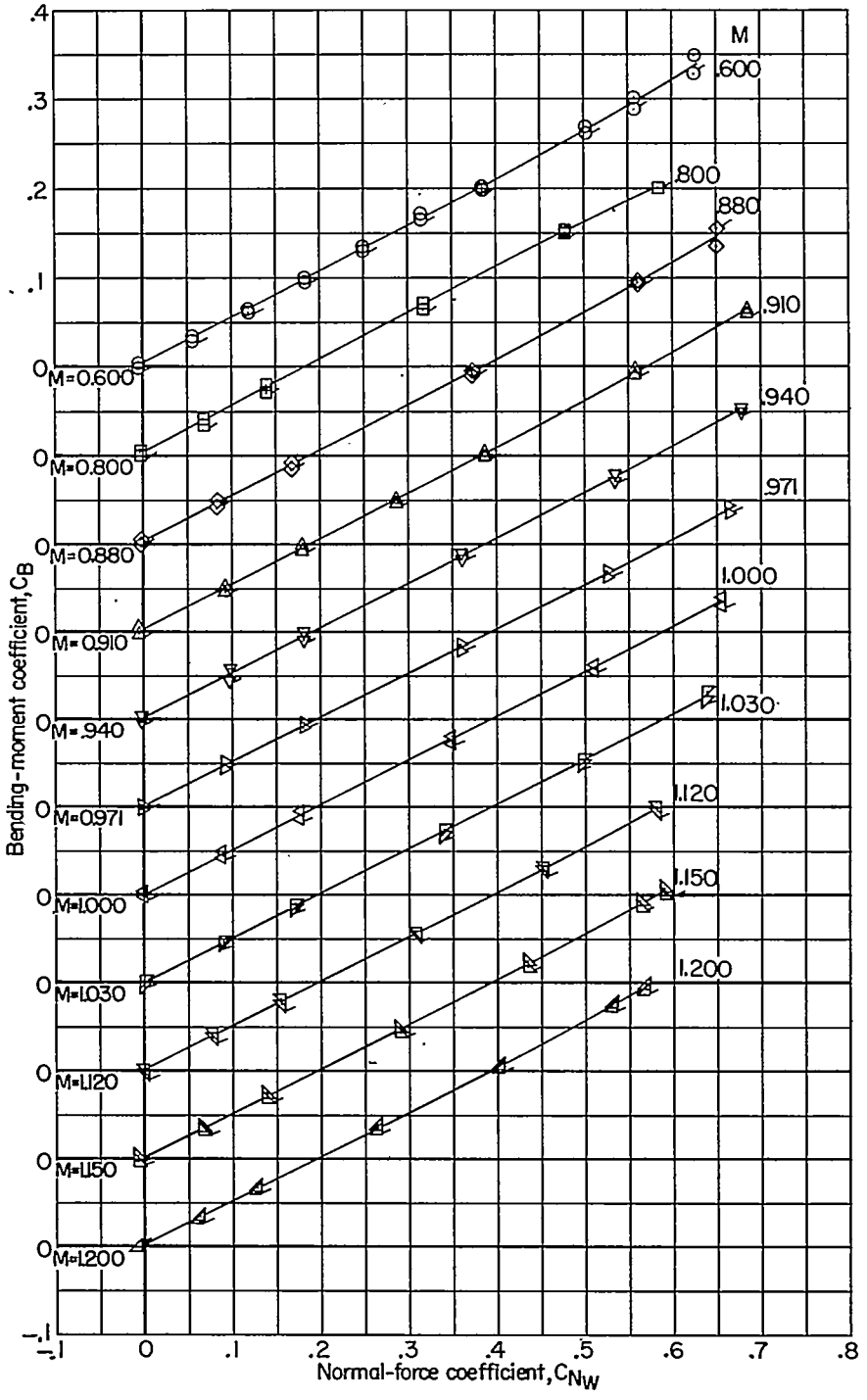

(c) Variation of C_B with C_{N_W} for left- and right-wing panels. Flagged symbols indicate left wing panel.

Figure 10.- Concluded.

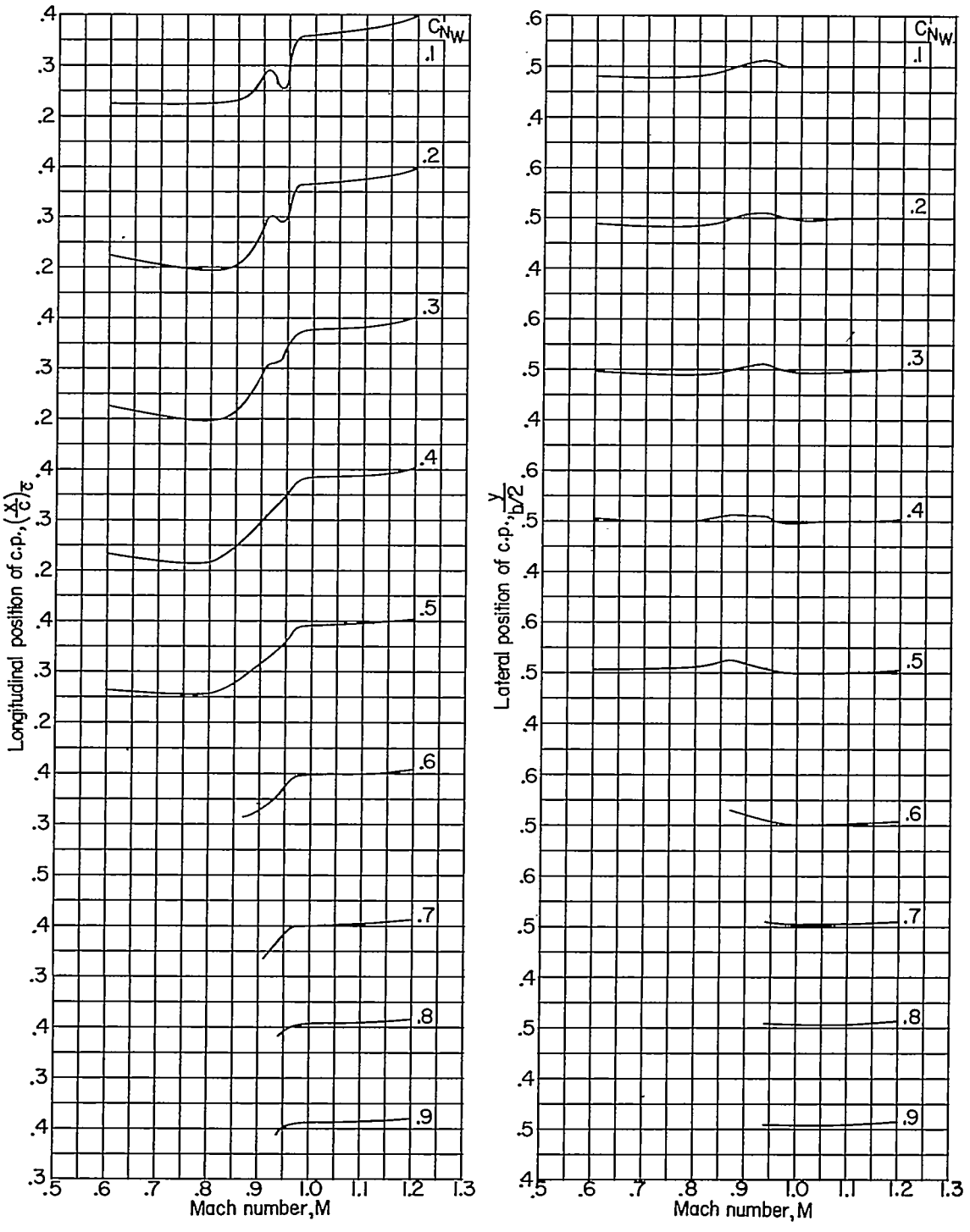

Figure 11.- Variation of the longitudinal and lateral location of the center of pressure with Mach number. 0° quarter-chord sweep; NACA 65A006 airfoil section.

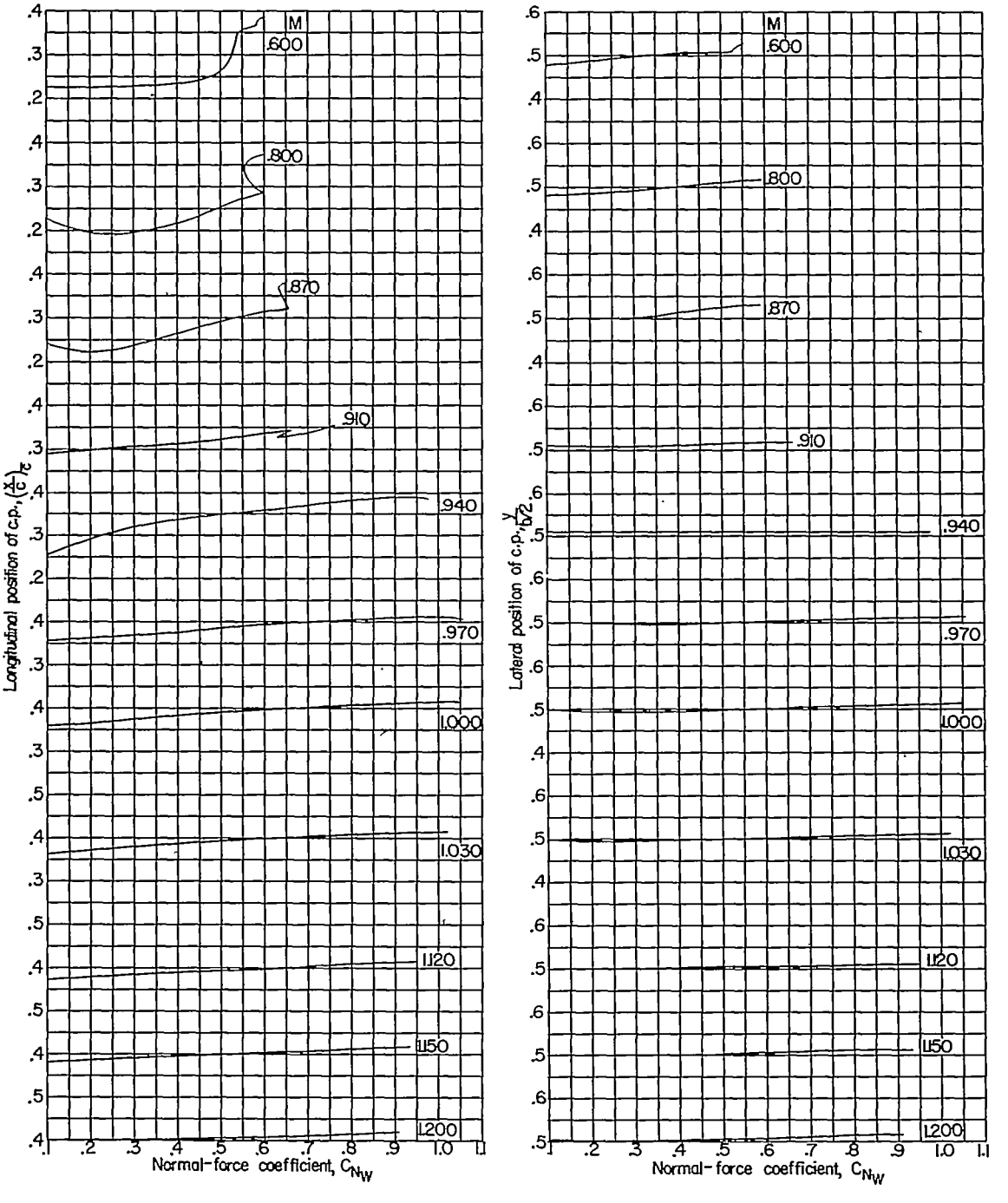

Figure 12.- Variation of the longitudinal and lateral location of the center of pressure with wing normal-force coefficient. 0° quarter-chord sweep; NACA 65A006 airfoil section.

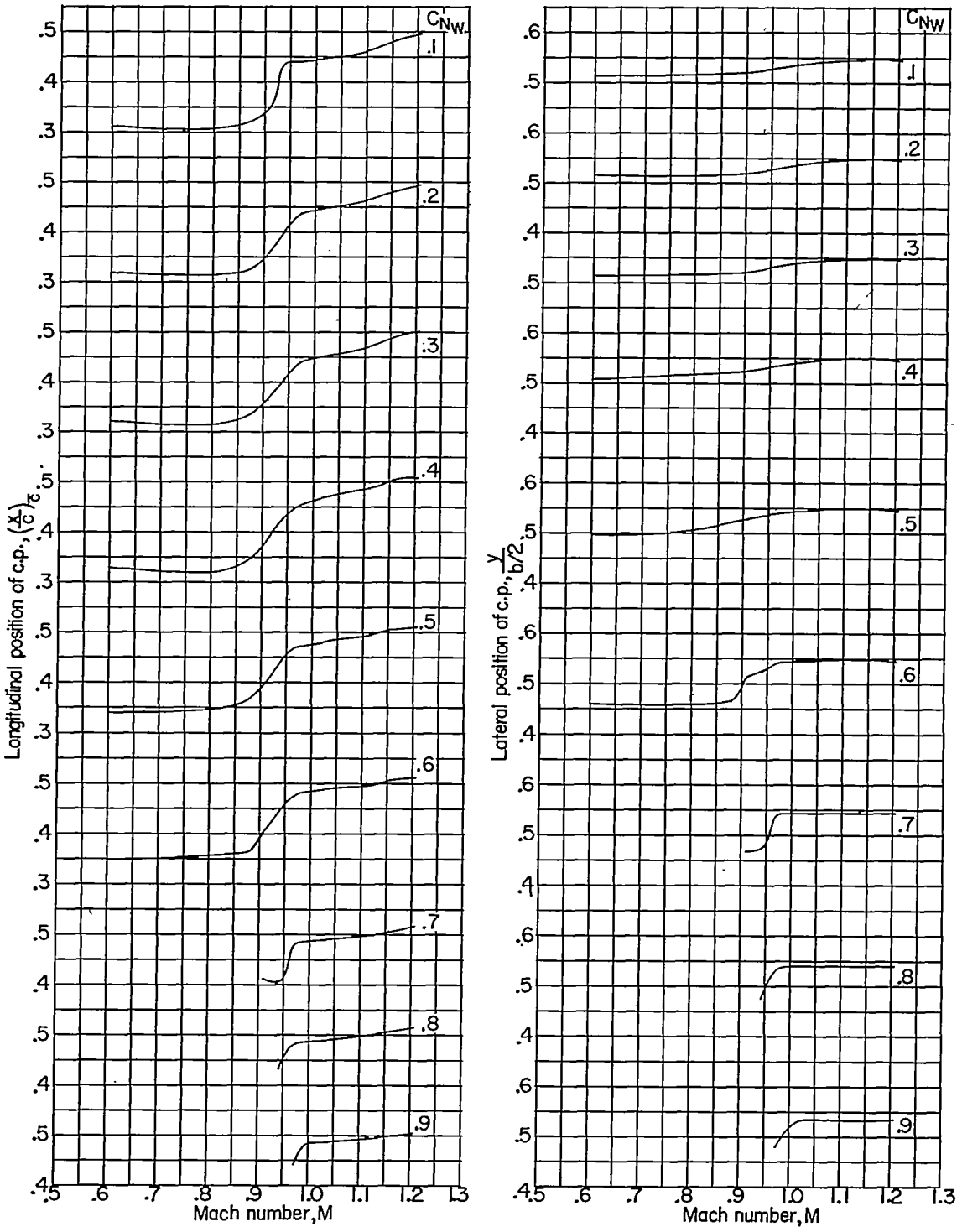

Figure 13.- Variation of the longitudinal and lateral location of the center of pressure with Mach number. 35° quarter-chord sweep; NACA 65A006 airfoil section.

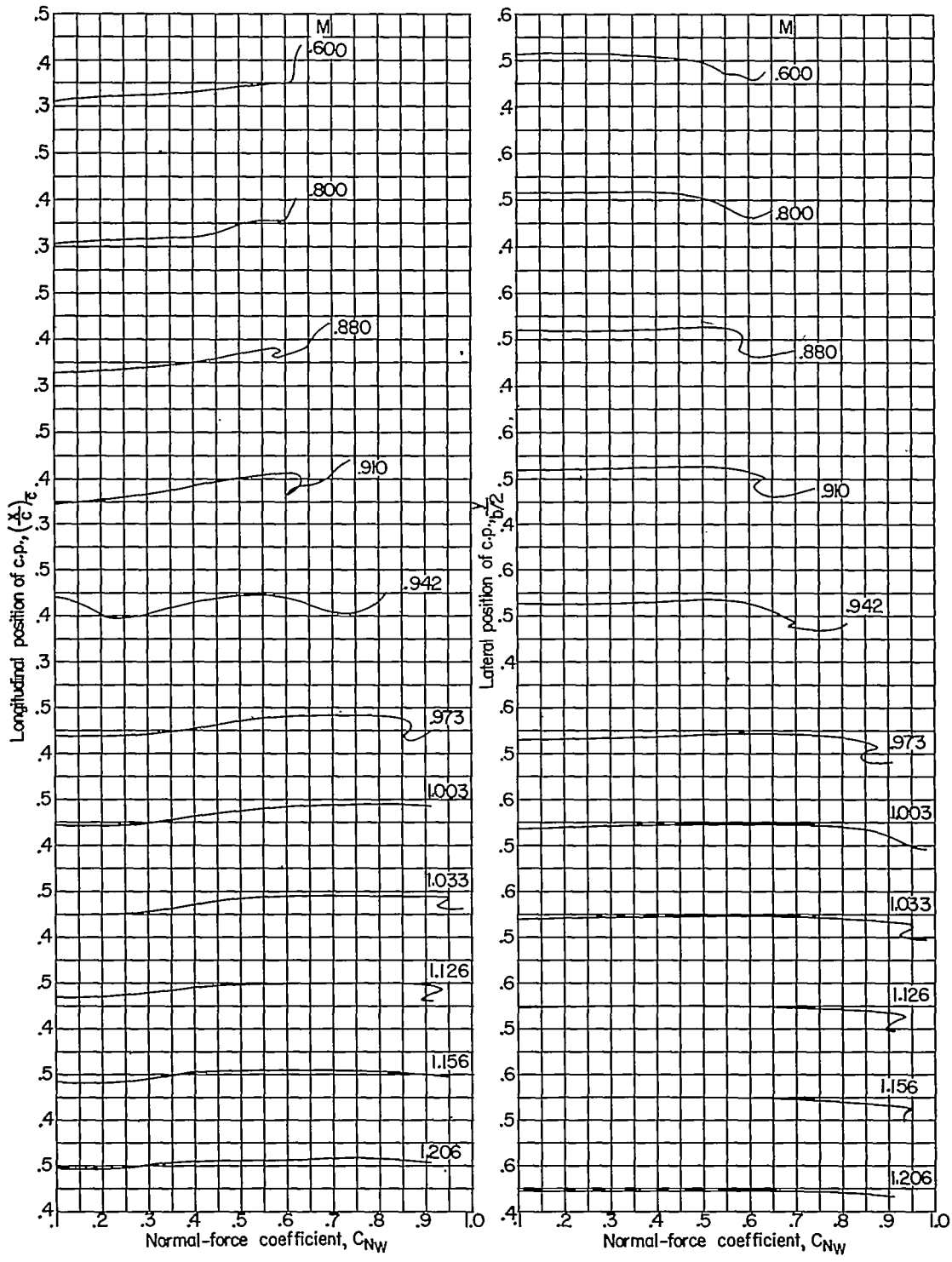

Figure 14.- Variation of the longitudinal and lateral location of the center of pressure with wing normal-force coefficient. 35° quarter-chord sweep; NACA 65A006 airfoil section.

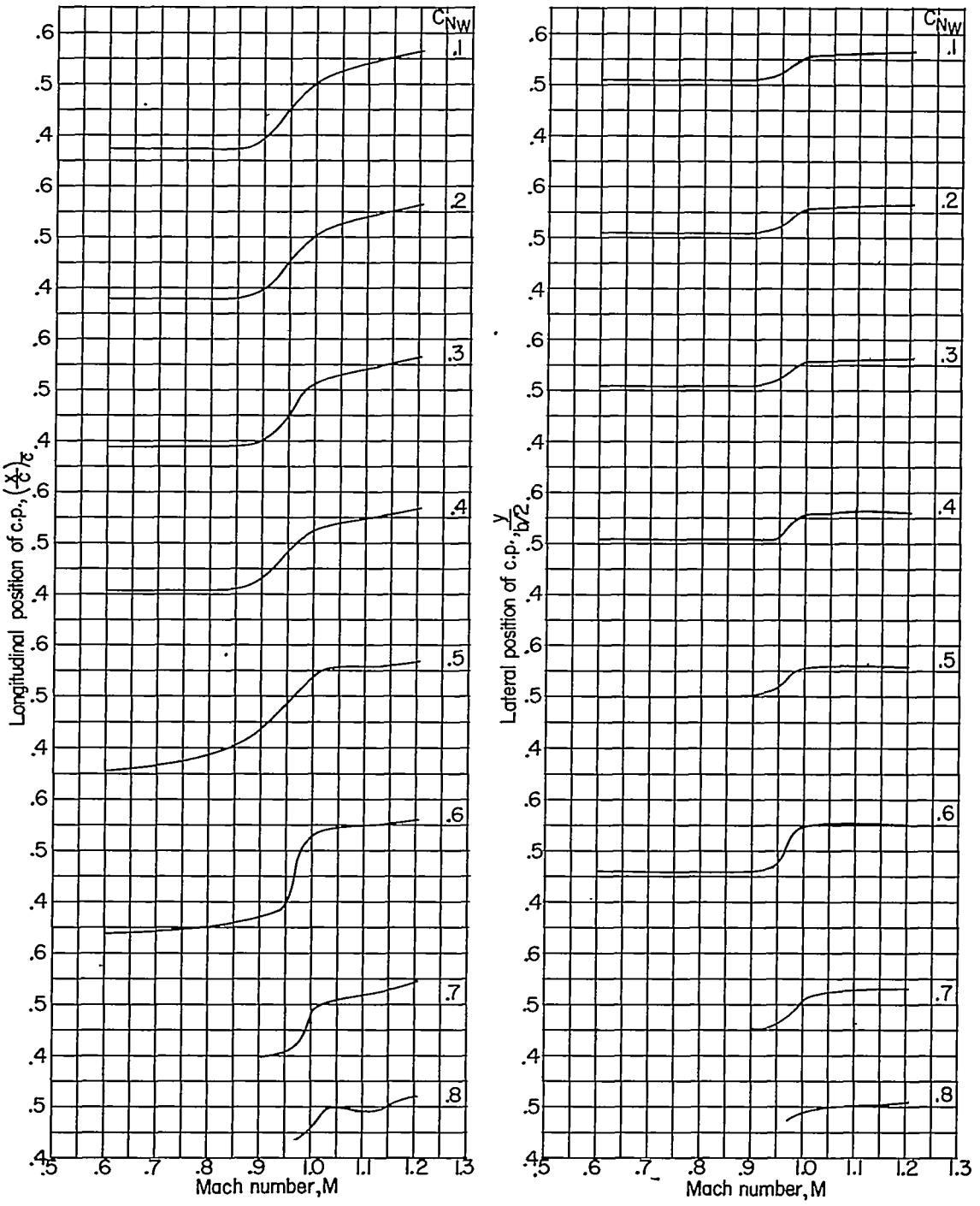

Figure 15.- Variation of the longitudinal and lateral location of the center of pressure with Mach number. 45° quarter-chord sweep; NACA 65A006 airfoil section.

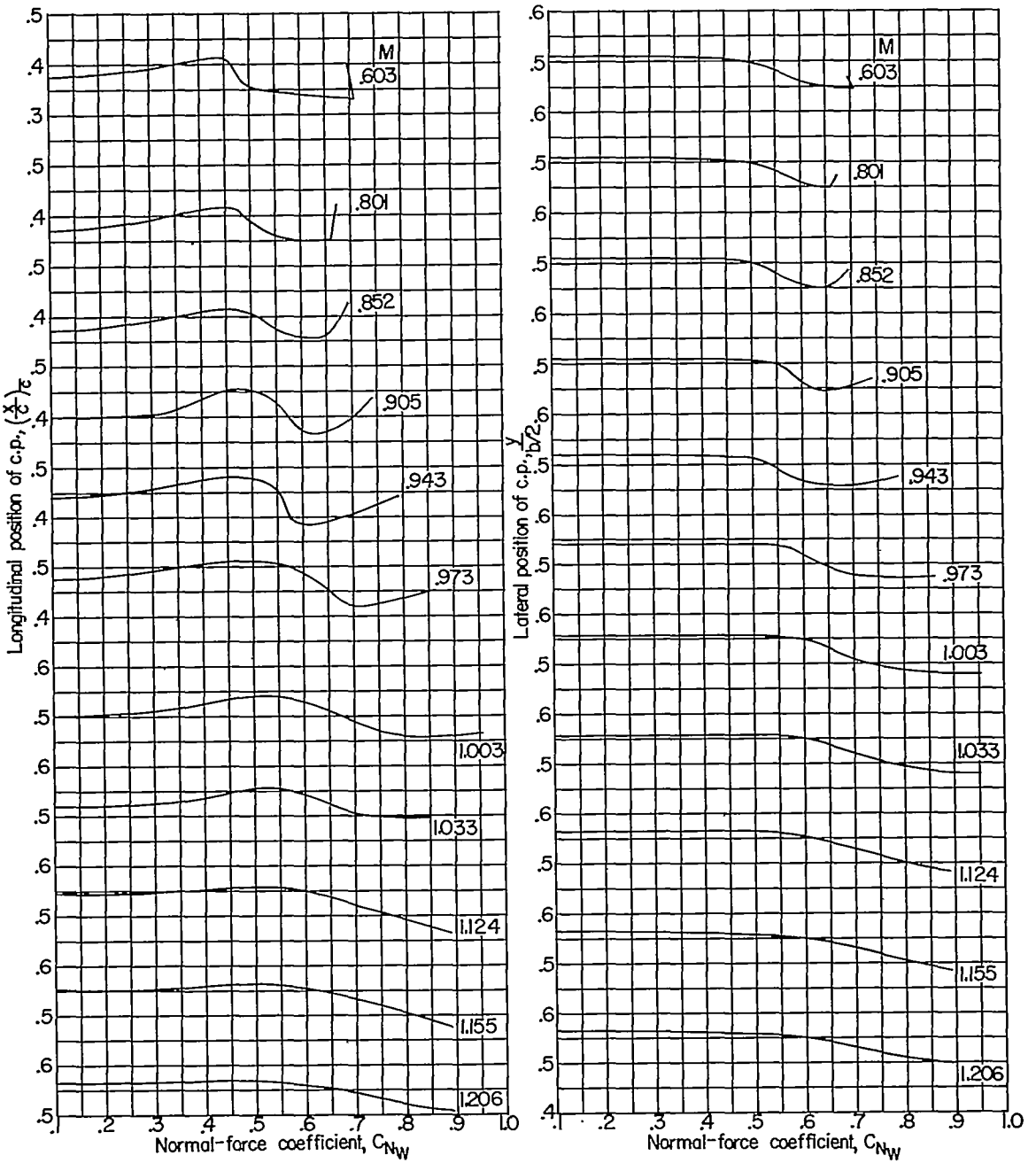

Figure 16.- Variation of the longitudinal and lateral location of the center of pressure with wing normal-force coefficient. 45° quarter-chord sweep; NACA 65A006 airfoil section.

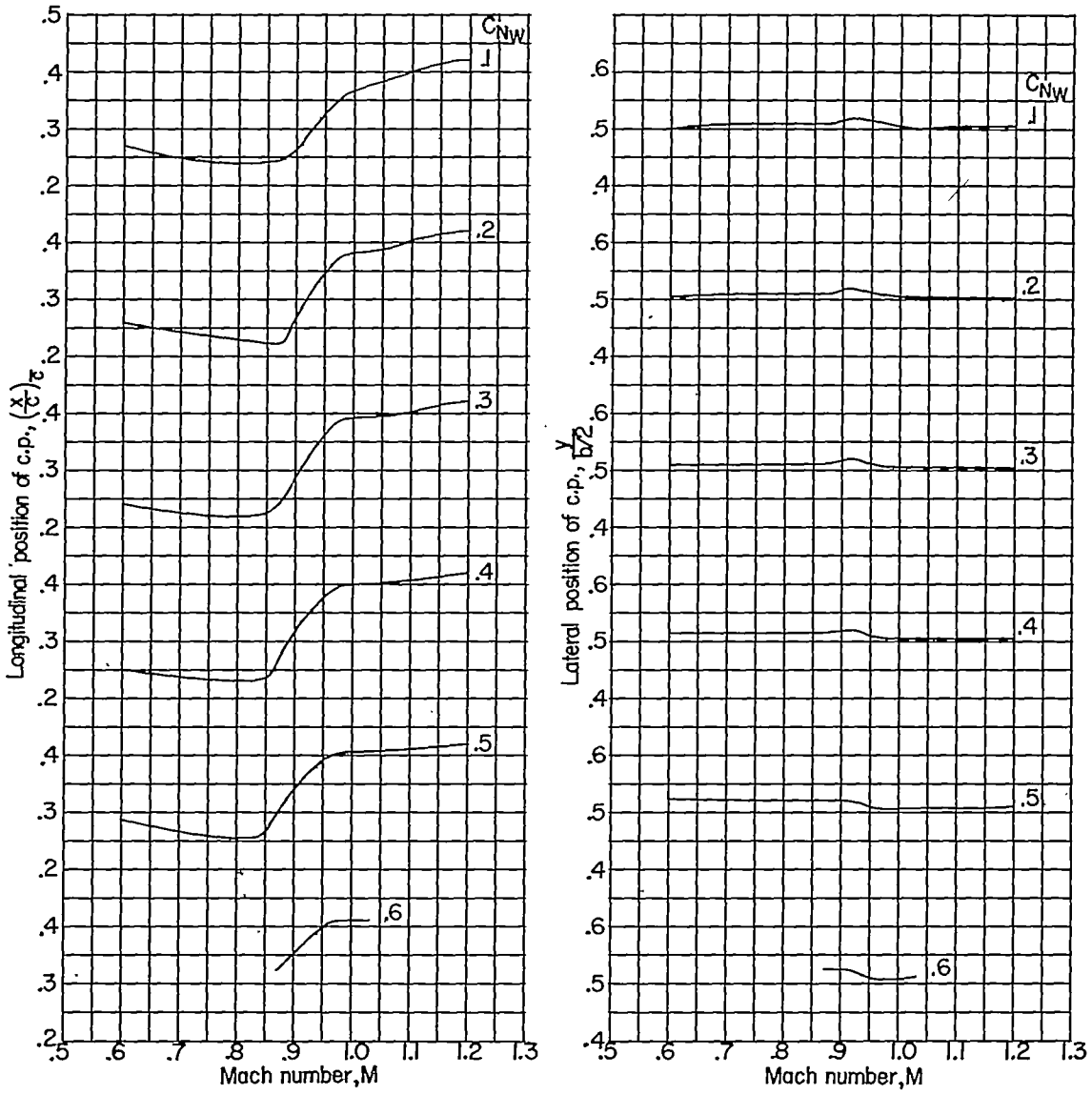

Figure 17.- Variation of the longitudinal and lateral location of the center of pressure with Mach number. 0° quarter-chord sweep; NACA 65A004 airfoil section.

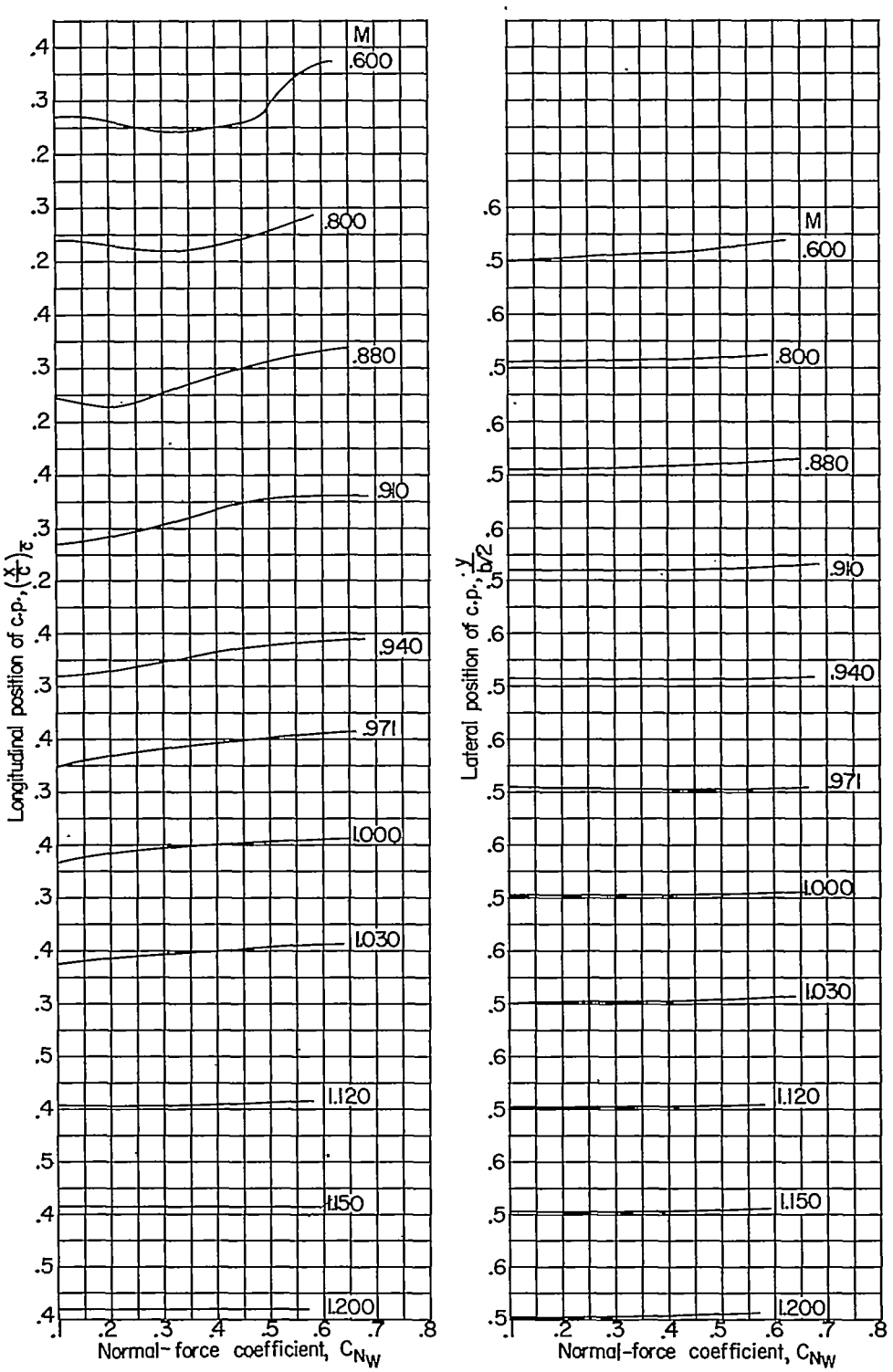

Figure 18.- Variation of the longitudinal and lateral location of the center of pressure with wing normal-force coefficient. 0° quarter-chord sweep; NACA 65A004 airfoil section.

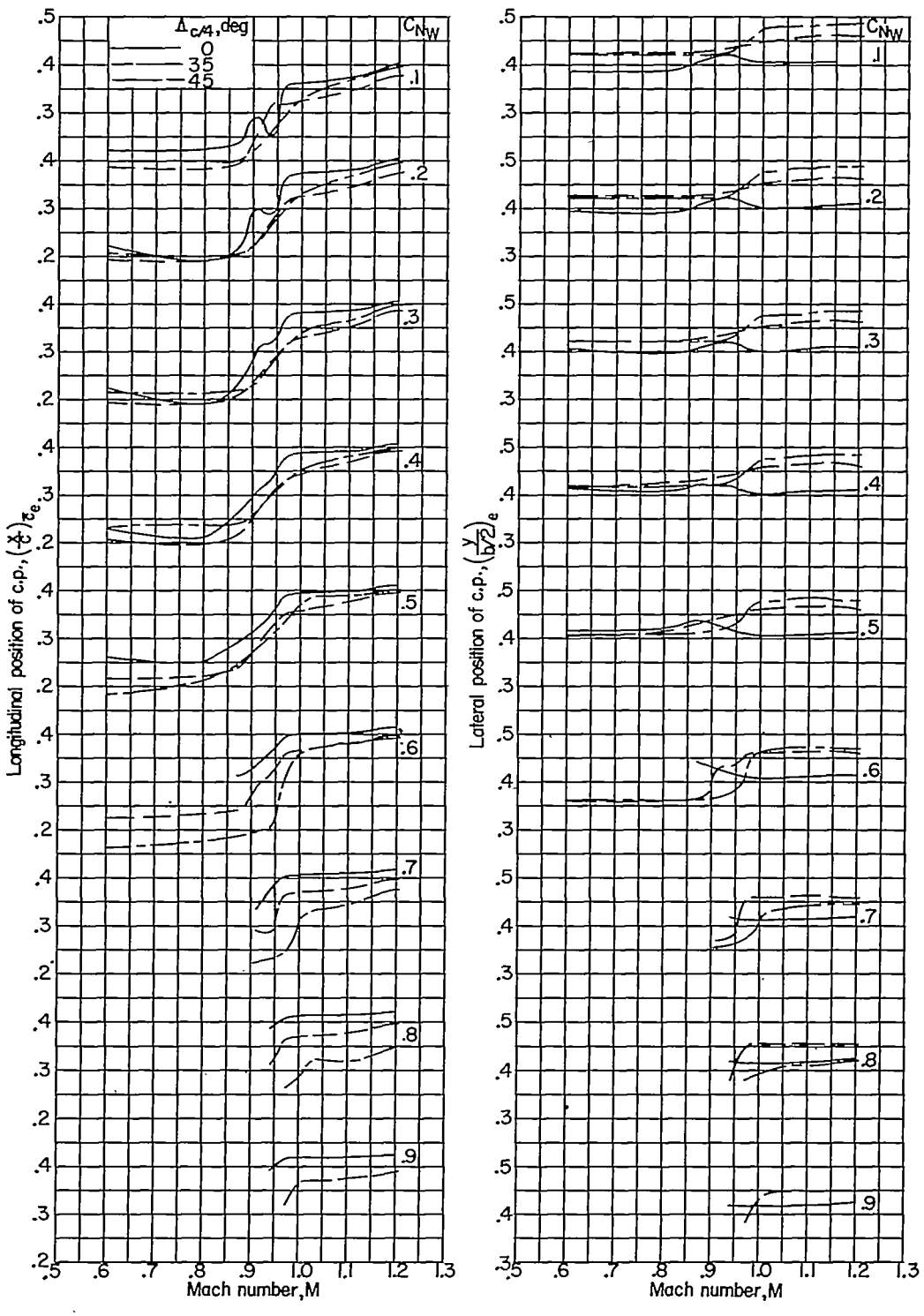

Figure 19.- Effect of sweepback on the variation of the longitudinal and lateral location of the center of pressure with Mach number. Center of pressure based on exposed wing. NACA 65A006 airfoil section.

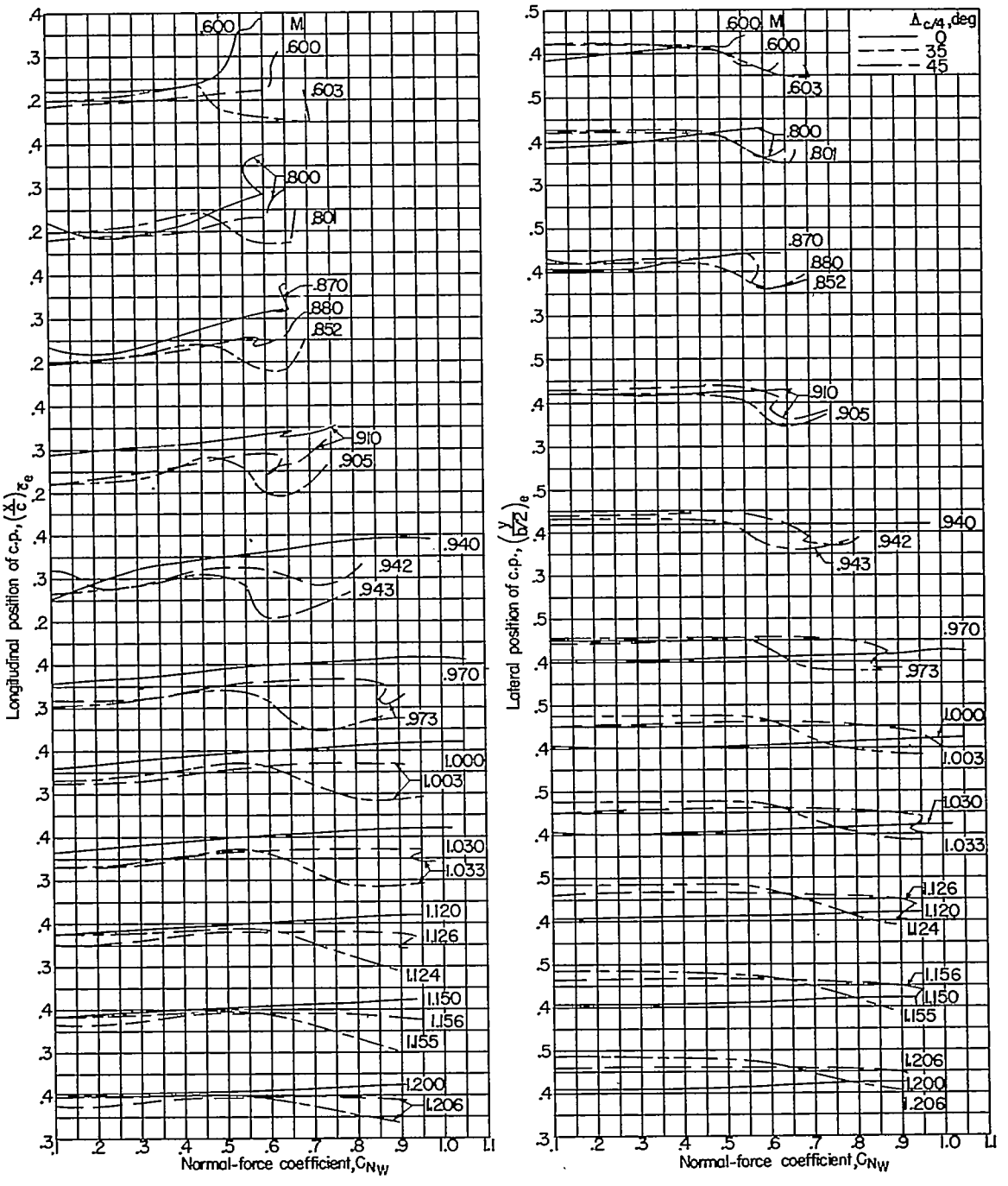

Figure 20.- Effect of sweepback on the variation of the longitudinal and lateral location of the center of pressure with wing normal-force coefficient. Center of pressure based on exposed wing. NACA 65A006 airfoil section.

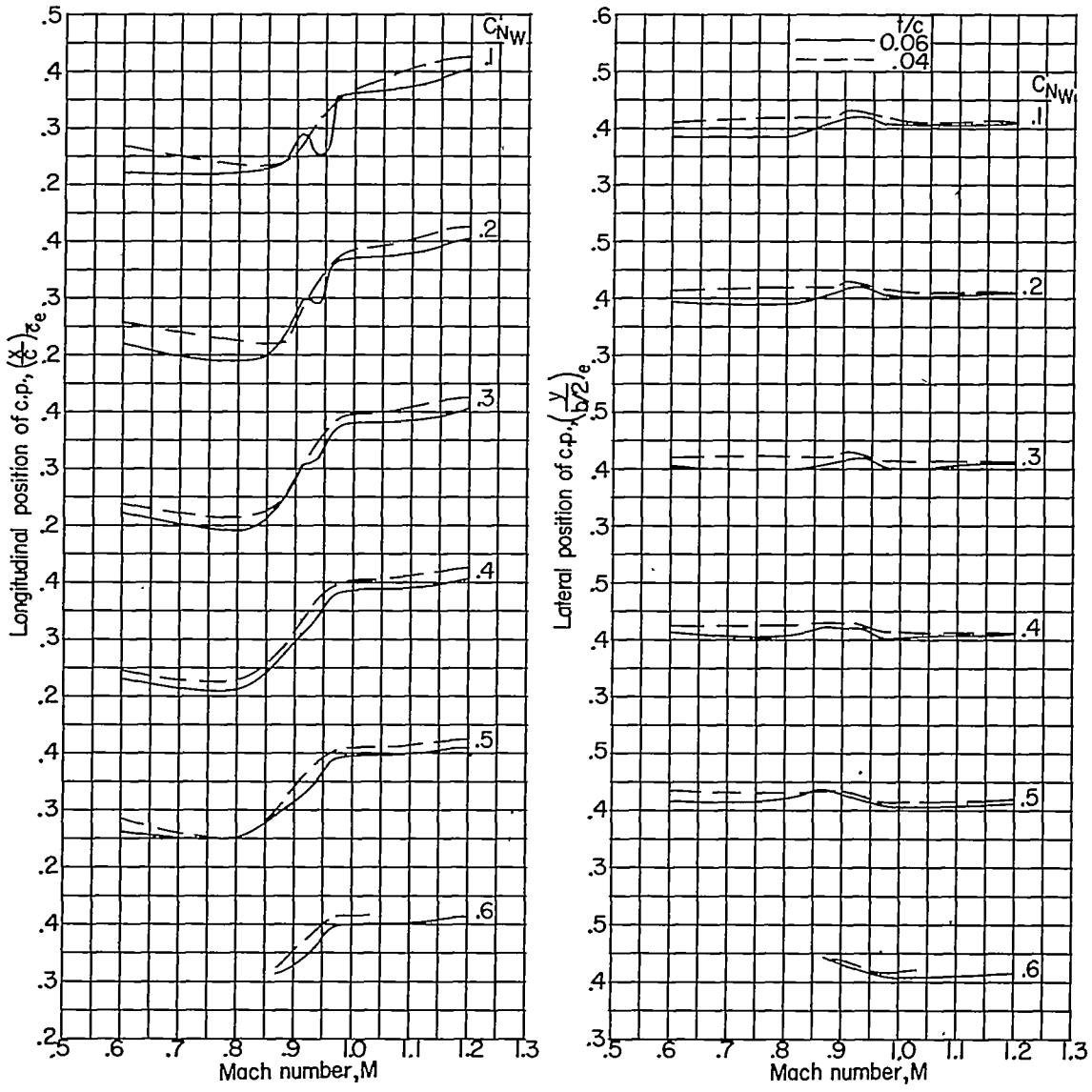

Figure 21.- Effect of thickness ratio on the variation of the longitudinal and lateral location of the center of pressure with Mach number. Center of pressure based on exposed wing. 0° quarter-chord sweep.

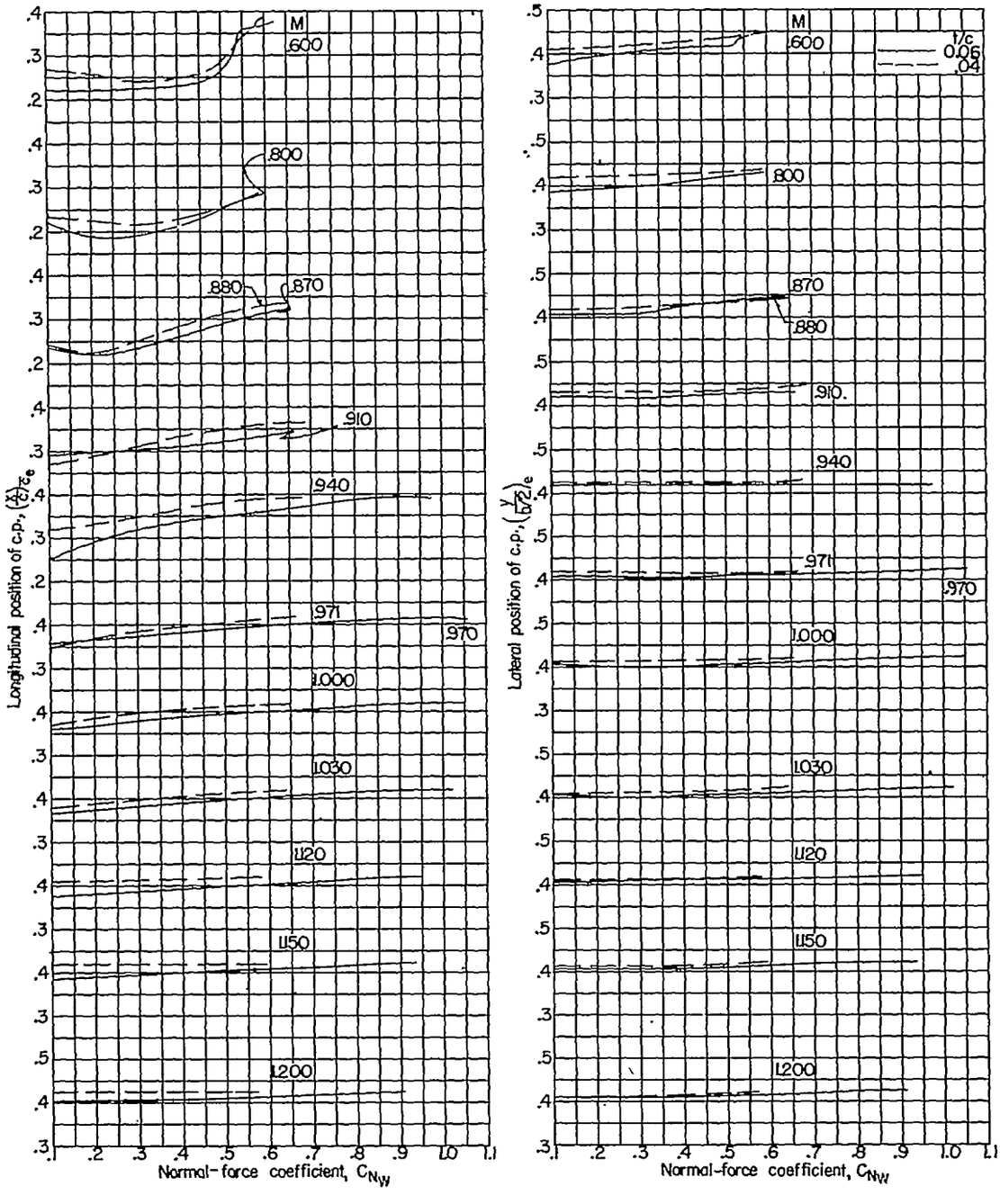

Figure 22.- Effect of thickness ratio on the variation of the longitudinal and lateral location of the center of pressure with wing normal-force coefficient. Center of pressure based on exposed wing. 0° quarter-chord sweep.

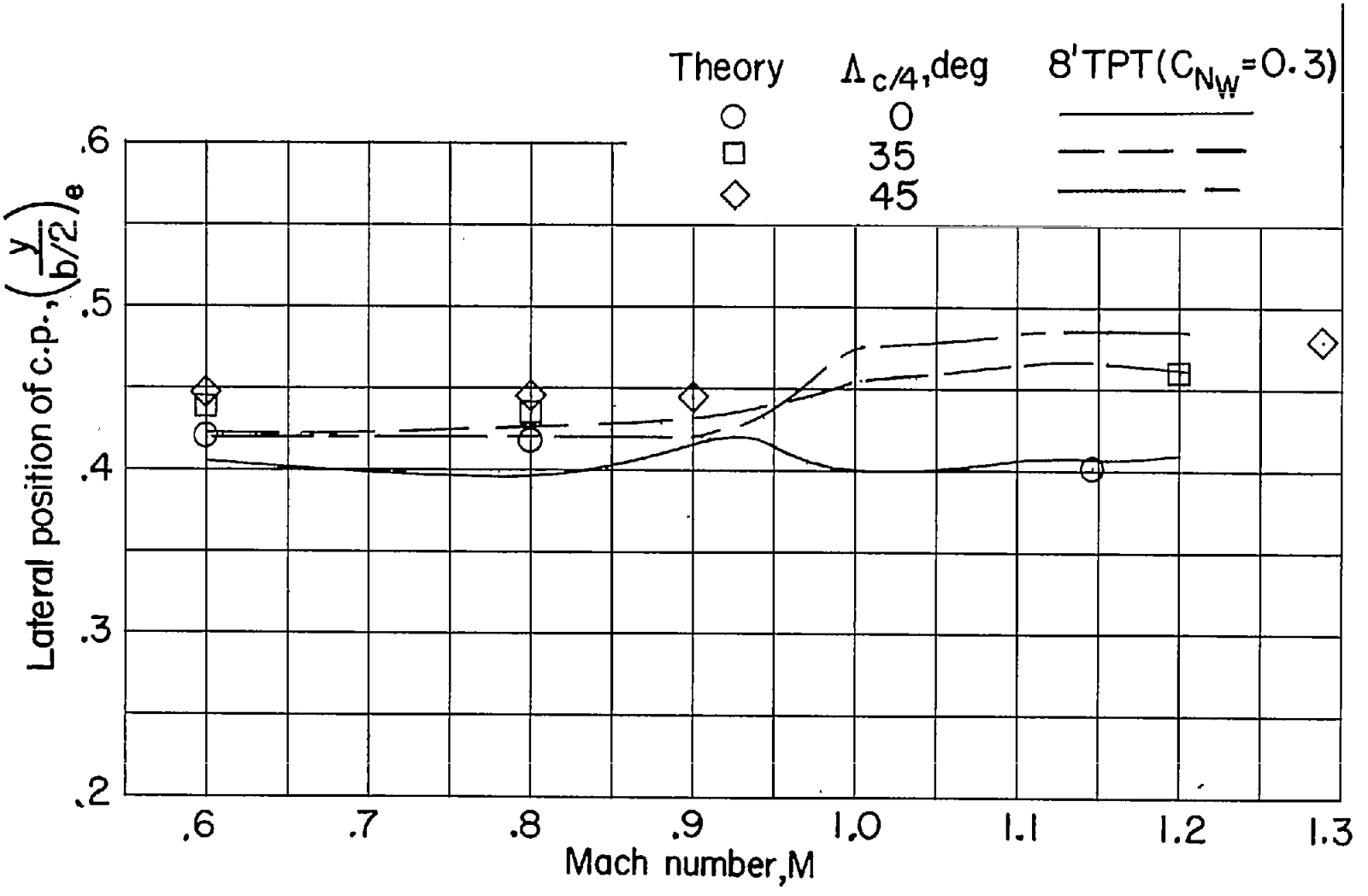

Figure 23.- Comparison of experimental lateral center-of-pressure location, based on exposed wing, with theory. Experimental data for wings with NACA 65A006 airfoil sections.